# Calibration of the electron volt spectrometer VESUVIO at ISIS

**J Mayers and M A Adams**

# 1. Introduction

The purpose of this report is to describe the procedures used to calibrate the VESUVIO spectrometer at the ISIS neutron source. VESUVIO is used primarily to measure the momentum distributions of atoms, by inelastic scattering of very high energy (5-150 eV) neutrons. This technique is known as neutron Compton scattering (NCS) by analogy with the older technique of Compton scattering, which is used to measure the momentum of electrons by scattering of high energy photons. Both techniques rely upon the fact that at sufficiently high momentum transfers, the impulse approximation (IA) is accurate [1]. The IA implies that the neutron scatters from a single atom, with conservation of kinetic energy and momentum of the neutron + atom. Hence the neutron inelastic scattering cross-section is related in a simple way to the momentum distribution of the atoms. Details of the technique and the data analysis used are given in references [2] and [3]. Examples of recent measurements made using VESUVIO are given in references [4,5,6,7,8,9,10].

VESUVIO is a unique instrument - other inelastic neutron spectrometers operate at energy transfers 2-4 orders of magnitude lower. Hence many of the calibration procedures used are also unique. An earlier paper [11] has already been published on this topic. However the instrument has recently been rebuilt with a different detection system and experimental geometry. Most of the calibration procedures described in this report are therefore new.

Section 2 contains a description of the current VESUVIO instrument and outlines the theory of the instrumental resolution. Section 3 discusses how the mean values of instrument parameters such as lengths, scattering angles and final neutron energy are determined at forward angles. Section 4 discusses the measurement of the distributions of these parameters about their mean values - these distributions determine the resolution of VESUVIO. Section 5 describes the procedures used to calibrate the detectors at back-scattering. Section 6 contains calculations of the resolution components of VESUVIO in momentum space for different atomic masses. Section 7 contains a summary and suggestions for future instrument improvements. Appendices 1-3 give details of the computer programs used in the calibration procedures. Appendices 4-6 give tables of the calibrated instrument parameters and the calibrated resolution parameters.

# 2. Description of VESUVIO

## 2a Instrument Layout

VESUVIO is illustrated schematically in Figure 1. There is a standard ISIS incident beam monitor (spectrum 1 or S1 in the data set) and a transmitted beam monitor (S2) composed of beads of $^6$Li doped scintillator glass.

At forward scattering there are 64 detectors (S135-S198) composed of cerium doped Yttrium Aluminium Perovskite (YAP) gamma ray detectors [12,13,14]. These are arranged in almost vertical columns of 8 detectors, with 4 above and 4 below the horizontal plane passing through the sample centre. Each detector element is 8cm in height, 2.5 cm in width and of thickness ~0.6 cm. Gold foils are placed on the surface of the detector and the gamma rays emitted due to the neutron absorption resonance at ~4.9 eV are detected. A differencing technique [15] is used to remove the background and sharpen the energy resolution. The final neutron energy is fixed at 4897 meV, with an energy resolution function which is well described by a convolution of a Lorentzian of HWHM 24 meV and a Gaussian of standard deviation 73 meV [16] (see section 4).

At back scattering there are 132 $^6$Li doped neutron detectors (S3-S134). A differencing technique with gold foils [17] is used to define the final energy as 4897 meV. Two different energy resolution functions are available at back-scattering. The single difference technique gives a broader resolution function than that obtained with the double difference technique [17], with correspondingly higher count rates.

## 2b Resolution Function of VESUVIO

Like all inelastic instruments at ISIS, VESUVIO uses time of flight measurements to determine the momentum and energy transfer to the neutron during each scattering event. The neutron counting chain assigns a time of flight $t$ to the arrival of each neutron at the detector:

$$t = \frac{L_0}{v_0} + \frac{L_1}{v_1} + t_0 \qquad (1)$$

$L_0$ is the path length from source to sample, $L_1$ that from sample to detector, $v_0$ is the velocity of the incident neutron and $v_1$ that of the scattered neutron. $t_0$ is an offset from the true value of $t$ due to delays in the electronic counting chain. On VESUVIO the values of $L_0$,

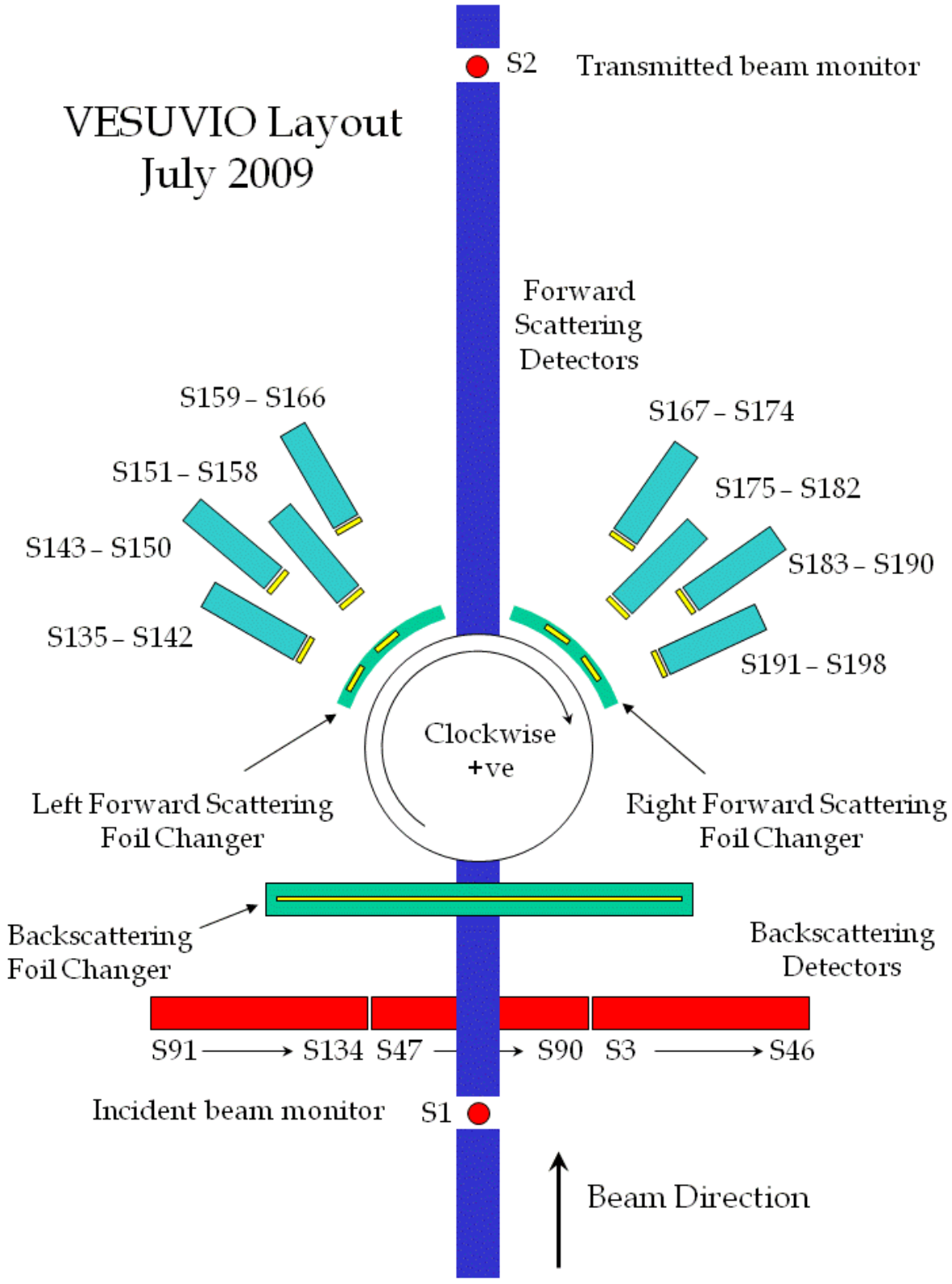


Figure 1. Schematic diagram of the VESUVIO instrument. The spectrum numbers corresponding to the different detectors are shown. The positions of the gold foils used in the differencing measurements are also indicated in yellow.

$L_1$, $v_1$, $t_0$ and the scattering angle $\theta$ can be characterised by a mean value, with an associated distribution about the mean. Given the mean values and the value of $t$ assigned to the neutron, the incident velocity $v_0$ of each neutron detected and hence the momentum and energy transfer in the scattering process can be determined from eq. (1).

The distributions about the mean values determine the resolution function of the instrument. The distribution in $L_0$ is determined by the finite size of the moderator and sample. The distributions of $L_1$ and $\theta$ are determined by the moderator, sample and detector geometry. The uncertainty in $v_1$ is determined by the band-width of energies absorbed by the gold foil. The uncertainty in the value of $t$ assigned to the neutron is determined by the time bin width and the stability of the electronics in the counting chain.

## 3. Determination of mean instrument parameters

### 3a Determination of the Incident Flight Path $L_0$

The incident flight path is determined by placing a uranium foil in the incident beam at the sample position. Uranium has a series of sharp neutron resonance absorption peaks. When a neutron is absorbed by one of these resonances, gamma rays are emitted and these are registered by the YAP detectors at forward scattering. One of the 64 YAP spectra obtained is shown in Figure 2.

When a neutron is absorbed by the foil, gamma rays are emitted effectively instantaneously and take a negligible time to pass from foil to detector. Hence the position in time of flight of the peaks in Figure 2 is determined by the time taken for neutrons to travel from source to foil. That is

$$t = \frac{L_0}{v_0} + t_0 \qquad (2)$$

The parameters describing the absorption cross-section of neutrons in uranium are very accurately known [18]. Hence given the known foil thickness, the absorption resonance can be accurately calculated at room temperature using the algorithm of reference [17]. The peak shapes are dominated by thermal broadening and are quite close to Gaussian. The calculated foil peaks were fitted to Gaussians to determine the neutron energy corresponding to the peak centres. The values obtained for the resonance energies and the

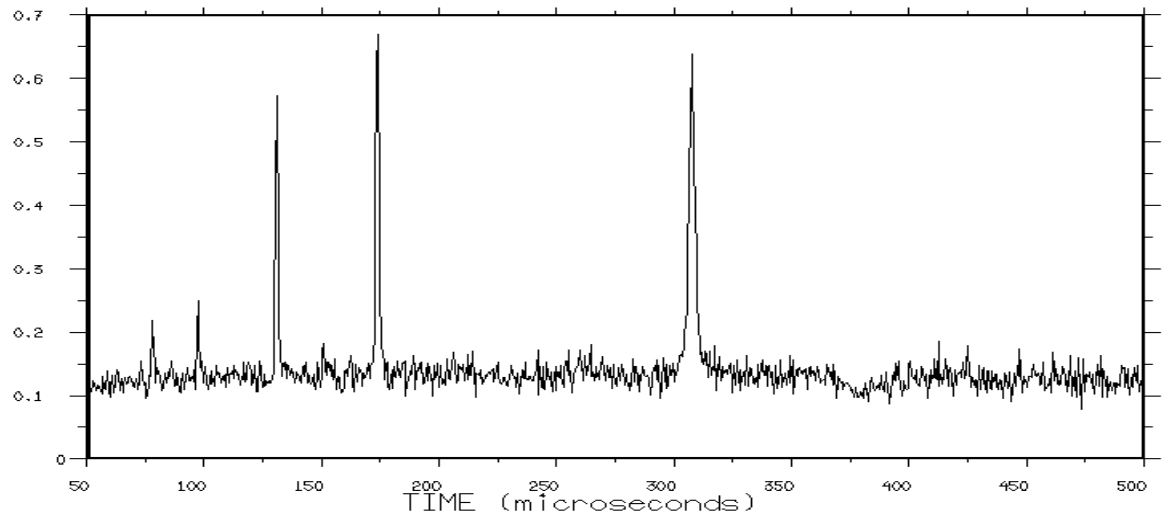


Figure 2. Resonance peaks observed in a single detector with a uranium foil at the sample position. The data was divided by the scattering from a lead sample to remove the spectrum shape.

standard deviation of the fitted Gaussians $\Delta E_R$ (the full width at half height is ~2.35 $\Delta E_R$) are listed in table 1. The measured peaks in the data shown in Figure 2 are also fitted to Gaussians in $t$. The final column of table 1 gives the fitted positions $t_R$ of the peaks in the time of flight data, averaged over the 64 YAP detectors. It follows from eq. (2) that if $t_R$ is

| $E_R$ (meV) | $\Delta E_R$ (meV) | $v_R$ (m/sec) | $t_R$ (μsec) |
|---|---|---|---|
| 6672 | 52.4 | 35725 | 307.70± 0.01 |
| 20874 | 91.7 | 63190 | 173.80± 0.01 |
| 36684 | 133.6 | 83768 | 131.00± 0.01 |

**Table 1.** Parameters defining the uranium absorption peaks used in the calibration. These were calculated for a foil with 1.2081 x $10^{20}$ atoms/cm$^2$. $E_R$ is the position of the Gaussian fit to the calculated absorption. $\Delta E_R$ is the fitted standard deviation. $v_R$ is the velocity of a neutron with energy $E_R$. $t_R$ is the mean fitted position in time of flight of the peaks shown in Figure 2, averaged over the 64 YAP detectors. The quoted error is the standard error in the mean over the 64 YAP detectors.

plotted as a function of $1/v_R$, the value of $L_0$ is obtained as the gradient and $t_0$ as the intercept. Figure 3a shows values of $L_0$ obtained from linear least-squares fitting of the three fitted peak positions in time of flight for the 64 YAP detectors. All detectors give the same

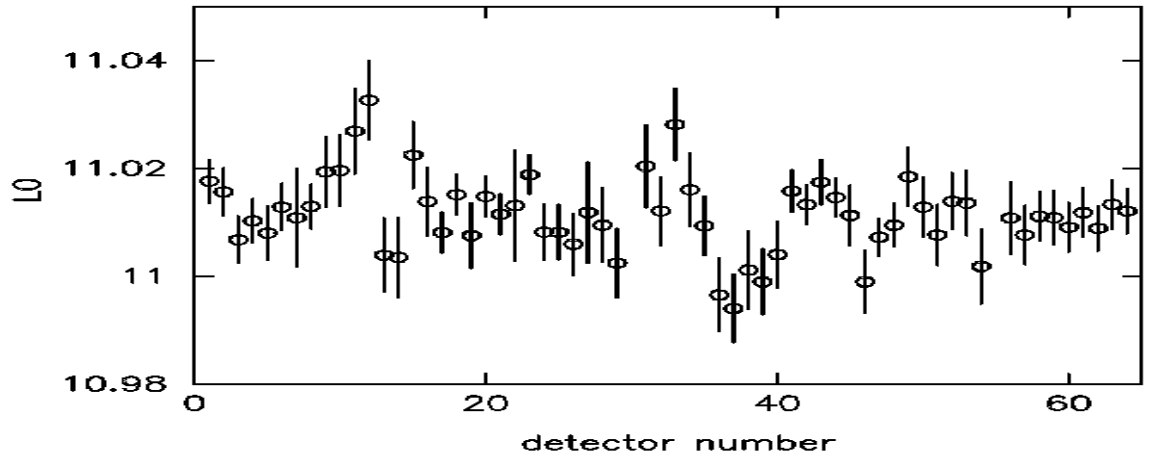


Figure 3a. Values of $L_0$ obtained from fitting the U resonance positions on the 64 YAP detectors at forward scattering angles. The mean of the 64 detectors is $L_0$ =11.005 ± 0.001 metres.

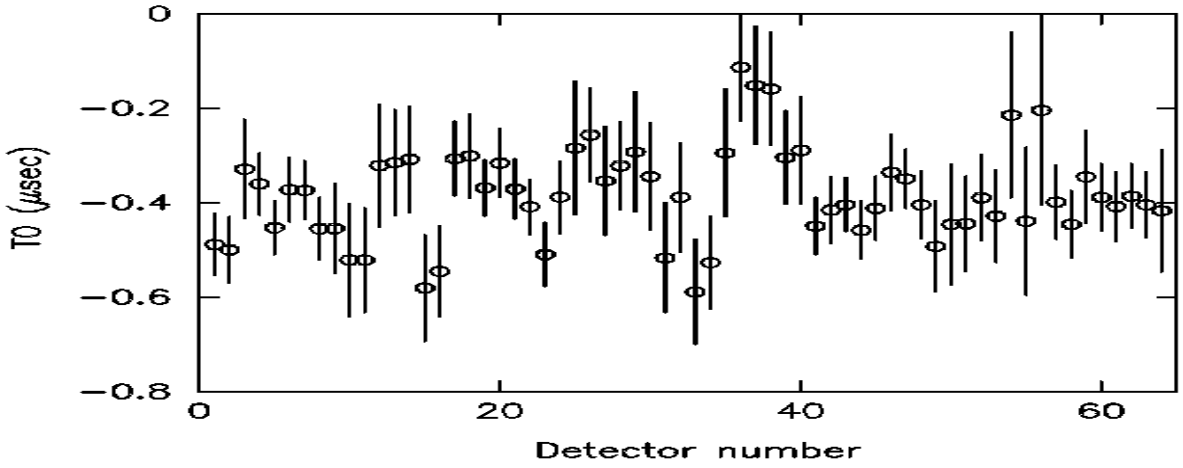


Figure 3b. Values of $t_0$ (μsec) obtained from fitting the U resonance positions on the 64 YAP detectors via the procedure described in the text. The mean is $t_0$ = -0.40 ± 0.02 μsec.

value of $L_0$ to within ~1cm. Figure 3b shows the corresponding values of $t_0$. The error bars in the plots are the standard errors in the fit to the 3 values. The mean over the 64 detectors of the incident flight path is $L_0$ =11.005 metres, with a standard error of ± 0.001 metres. The mean value of the time delay is $t_0$ = -0.40 μsec with a standard error of ± 0.02 μsec. The negative value of $t_0$ implies that the time zero pulse arrives at the detector electronics after

the mean time of emission of the neutrons. This is presumably due to electronic delays in the counting chain.

### 3b Determination of the Final Energy $E_1$

The mean final energy $E_1$ of the neutron was determined using the $^6$Li doped back-scattering detectors. Figure 4 shows a typical time of flight spectrum collected on one of these detectors with the standard VESUVIO lead calibration sample. This is a 2mm thick slab, which scatters about 7% of the beam. Lead is a good calibration standard for NCS measurements for a number of reasons. It has a low Debye temperature (90 K) and hence behaves essentially as a non-interacting Maxwell-Boltzmann gas at room temperature [19]. It therefore has a momentum distribution which is closely Gaussian. Partly due to its low Debye temperature and partly to its high mass the lead peak is much narrower than the resolution function of the instrument, as can be seen from Figures 4 and 6. The scattering is also very close to isotropic and elastic due to the high mass of lead and the correspondingly small recoil.

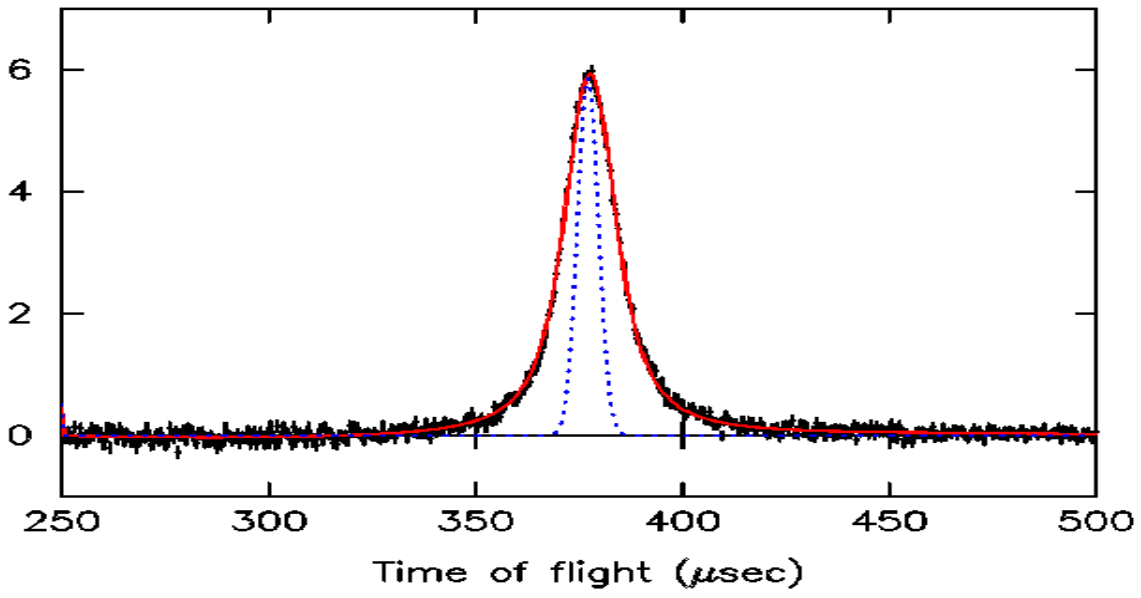


Figure 4. The black points are a typical time of flight spectrum from one of the 132 $^6$Li doped detectors (at ~140 degrees), with the lead calibration sample. The Voigt fit to the data is shown as the red line. The calculated width in $t$ due to the momentum distribution of the lead atoms is shown as the blue dotted line.

At the energies of the uranium resonances, calculations [19] show that the IA is very accurate for scattering from lead at room temperature. Hence the ratio of the final and incident neutron velocities of neutrons detected at the peak centre (corresponding physically

to an atom with zero momentum) is accurately fixed by conservation of kinetic energy and momentum of the neutron + atom as

$$\frac{v_1}{v_0} = \frac{\cos\theta + \sqrt{(M/m)^2 - \sin^2\theta}}{(M/m)+1} \qquad (3)$$

where $M$ = 207.19 amu. is the mass of a lead atom, $m$ = 1.0087 amu is the mass of the neutron and $\theta$ is the scattering angle.

A typical fit of a Voigt function (a convolution of a Lorentzian and a Gaussian) to the time of flight lead data is shown in Figure 4. The values of $L_0$, $L_1$, $t_0$ and $\theta$ can be calibrated very precisely on the $^6$Li doped detectors, using the methods given in ref [11] and applied in section 5. Hence using eqs. (1) and (3) and the fitted positions of the lead peak in time of flight, the value of $v_1$ and hence $E_1 = \frac{1}{2}mv_1^2$ can be determined from each detector. The values of $E_1$ obtained from averages over the three back-scattering banks are given in table 2.

| Detector bank | $E_1$ (meV) |
|---|---|
| S3-S46 | 4897.1 ± 0.7 |
| S47-S90 | 4897.5 ± 0.7 |
| S91-S134 | 4895.6 ± 0.8 |
| S3-S134 | 4897.3 ± 0.4 |

**Table 2.** The values of the mean final energy $E_1$ obtained from fitting lead data at back scattering. The errors are the standard error in the mean.

The foil absorption was also calculated for the known gold foil thickness used on VESUVIO. The algorithm given by reference [17] and tabulated parameters from reference [18] were used. The calculated foil absorption is shown in Figure 5, as the black dots. The calculated absorption was fitted with a Voigt function and gave a value of $E_1$ = 4906.4 meV for the peak position. The fit is shown as the red line. A fit to the square of the absorption (this is the resolution function at forward scattering [16]) gave an identical value for $E_1$.

The quoted errors [18] on the parameters used in the calculation give an error in the peak position of ± ~10 meV. Hence within error the calibrated value of $E_1$=4897 meV agrees with the value of 4906 meV obtained from the calculation. The calibrated value is

preferred as it should be more accurate - it is determined essentially by the tabulated values of the positions of uranium resonances, which are known much more accurately than those of gold (to within ± ~1meV [18] ). The value of $E_1$ used for the YAP detectors is the average over the values obtained from the back-scattering detectors of 4897.3 meV.

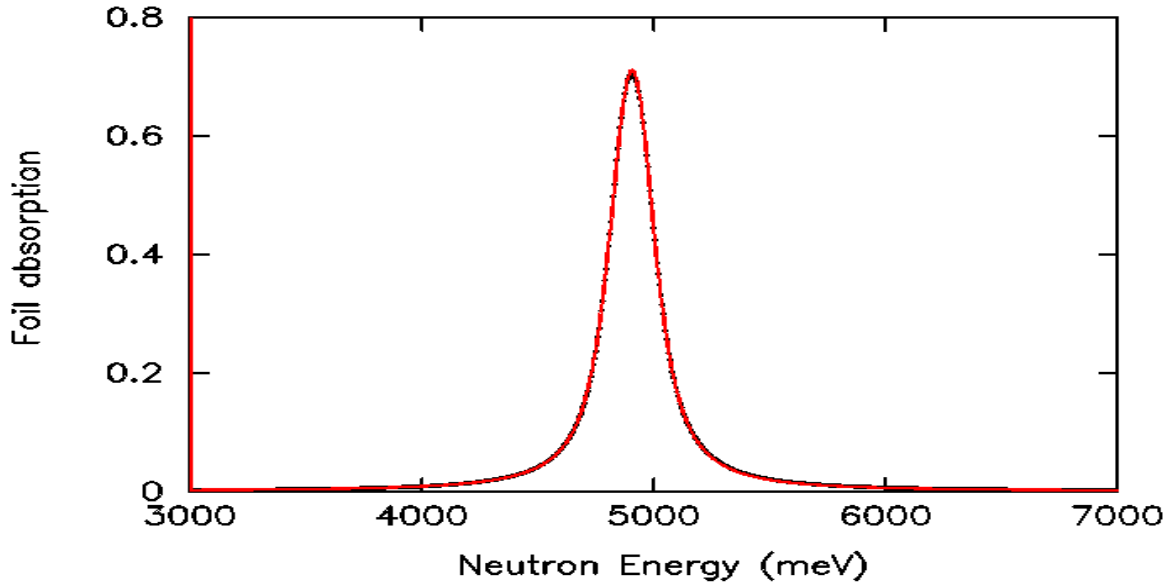


Figure 5. Calculated foil absorption is shown as the black dots. The fit of a Voigt Function is shown as the red line. The fitted peak position was 4906.4 meV.

### 3c Determination of the Final Flight Path $L_1$

The final flight path from sample to detector can also be determined from the lead calibration. The time of flight data in every YAP detector is fitted to a Voigt function after correcting for gamma background [20] and multiple scattering [21]. Typical data and the fit for a single YAP detector are shown in Figure 6. Given the calibrated values of $L_0$, $t_0$ (section 3a) , $v_1$ (section 3b) and $\theta$ (section 3d), $L_1$ can be determined by use of eqs. (1) and (3). Values of $L_1$ determined in this way are shown for the 64 YAP detectors in Figure 7. The statistical error in the calibrated value of $L_1$ for each detector is ~1mm.

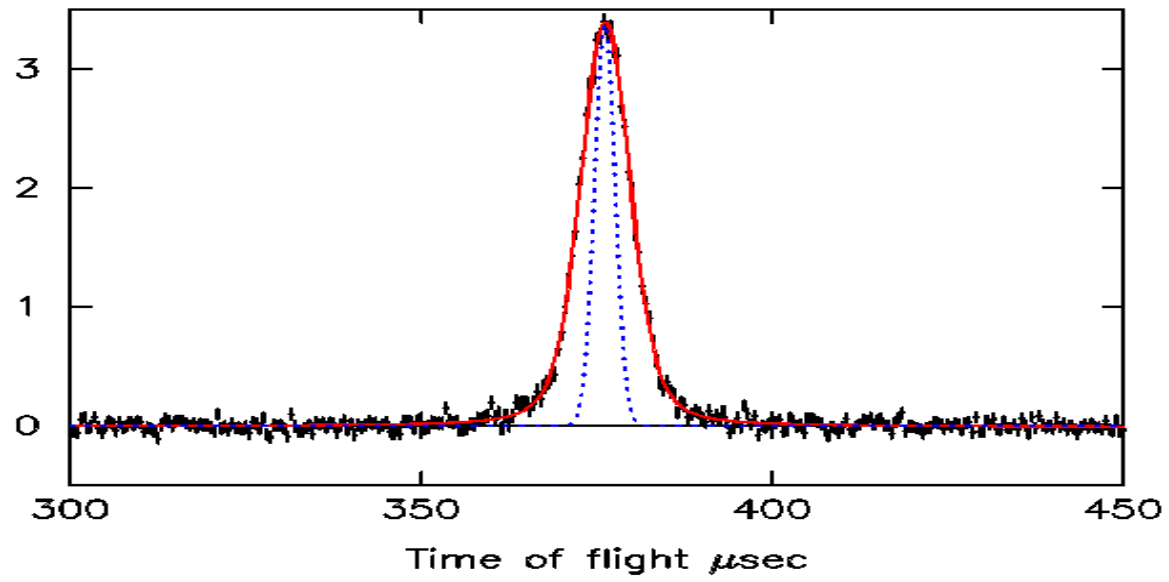


Figure 6. The scattering from lead in a single YAP detector (at ~50 degrees) after correction for gamma background and multiple scattering. The data is shown in black with statistical errors. The red line is a fit to a Voigt function. The blue dotted line is the intrinsic width due to the calculated lead momentum distribution at 290 K.

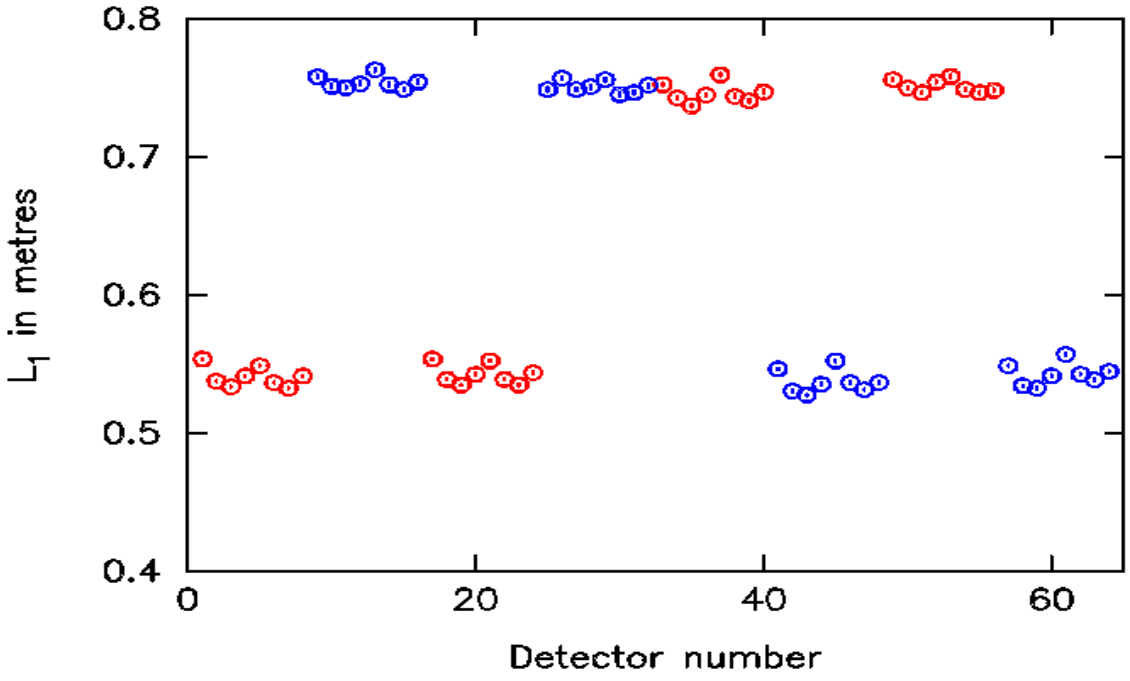


Figure 7. The values of $L_1$ in metres determined for the 64 YAP detectors at forward angles.

### 3d Determination of the Total Scattering Angle

The YAP detectors are covered with a thin foil of cadmium which absorbs neutrons in the thermal region. The gamma ray emission associated with this absorption allows the detection of neutrons with energies <200 meV. Scattering from lead therefore produces Bragg peaks. A typical spectrum showing the 5 longest d-spacing Bragg peaks of lead is shown in Figure 8.

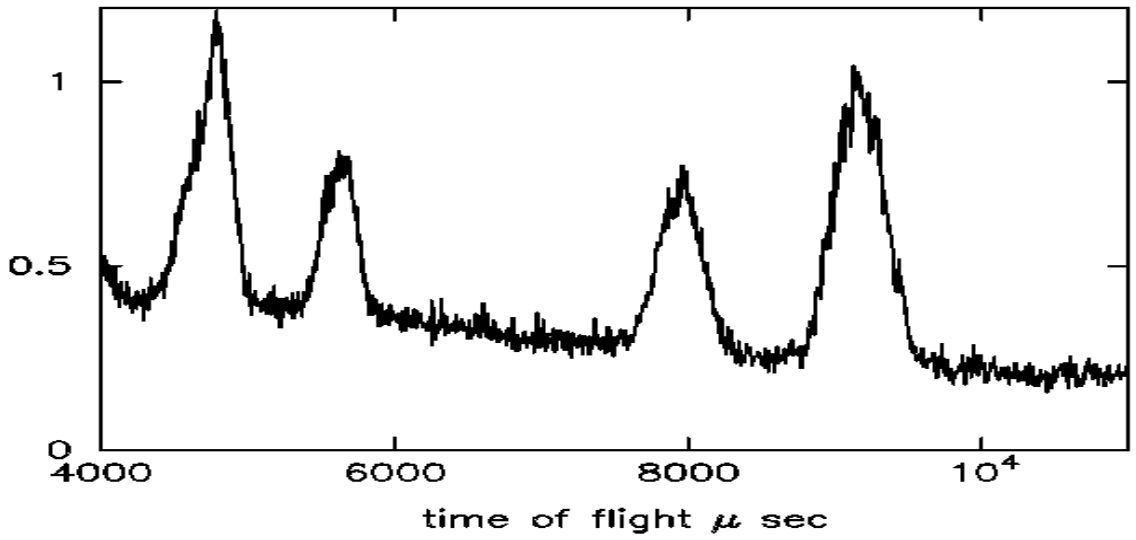


Figure 8. The 5 longest d-spacing Bragg peaks from lead at a scattering angle of 50 degrees. The peak at ~4600 μsec is the superposition of two peaks which are not resolved.

According to Bragg's law, the scattering angle is given by

$$2d\sin\theta = \lambda \qquad (4)$$

The d-spacings for lead can be calculated from tabulated values of the lattice parameter. The neutron wave length, $\lambda$, is determined by the time of flight at the peak centre and the calibrated values of $L_0$, $L_1$ and $t_0$ obtained via the procedures in sections 3a and 3c. Hence the scattering angle $\theta$ can be determined from eq. (4)[1].

[1] Since the values of $\theta$ are required to determine $E_1$ and $L_1$ and vice versa, the procedure may seem inconsistent. However $E_1$ and $L_1$ depend only very weakly upon $\theta$ and accurate values can be obtained by an iterative procedure: (1) Use estimated value of $\theta$ to determine $E_1$ and $L_1$, (2) with these values of $E_1$ and $L_1$, determine new value of $\theta$, (3) with new value of $\theta$ re-determine $E_1$ and $L_1$ etc. The procedure converges within a single iteration.

The positions of the 4 Bragg peaks with longest d-spacing in each of the 64 detectors were determined in the time of flight spectra using a cursor. The scattering angle is taken as the mean of the 4 values of $\theta$ determined from these positions. Figure 9 shows mean values of $\theta$ determined by this method. The standard error in the mean of the 4 values is typically ± ~0.2 degrees for each detector.

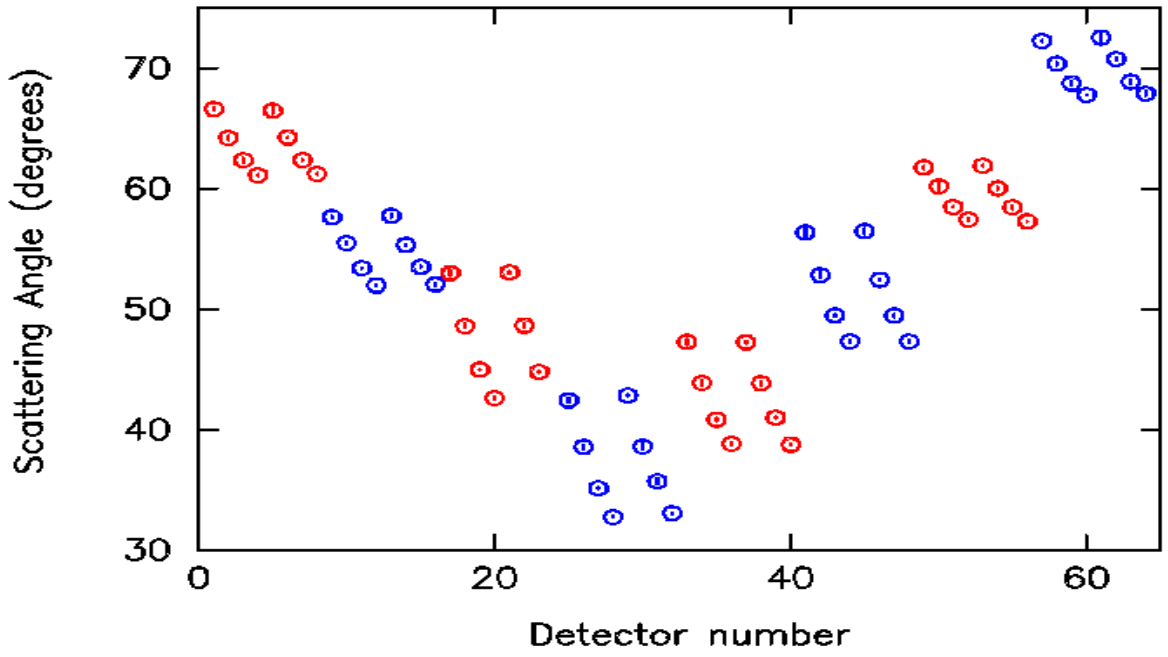


Figure 9. The values of the total scattering angle obtained from the calibration for the 64 YAP detectors.

The systematic change in scattering angle in banks of 4 detectors, which can be observed in Figure 9 is due to the fact that the YAP detectors are in vertical columns of 4 above and below the horizontal plane containing the sample. As the distance of the detector from this plane increases, the scattering angle also increases.

**3e Comparison with Direct Measurement**

The positions of the detectors were also measured directly using a combination of steel rules and a purpose built protractor consisting of a lid on top of the sample environment bin and a straight edge which could rotate about the sample centre.. From these measurements the total scattering angle $\theta$ and the final flight path $L_1$ can be calculated and compared with those obtained by the calibration procedures given in sections 3a-3d. The differences between the values of $L_1$ obtained by the calibration procedure and direct

measurement are shown in Figure 10a, while the difference in the calibrated and directly measured scattering angles $\theta$ are shown in Figure 10b.

It can be seen that there is generally good agreement between the direct measurement and the calibrated values. The lengths $L_1$ agree to within ~1 cm and the angles to within ~1º. The most probable origin of the discrepancies is a slight misalignment of detectors. This makes the determination of $L_1$ and $\theta$ by direct methods difficult, although these parameters can still be precisely determined by neutron calibration.

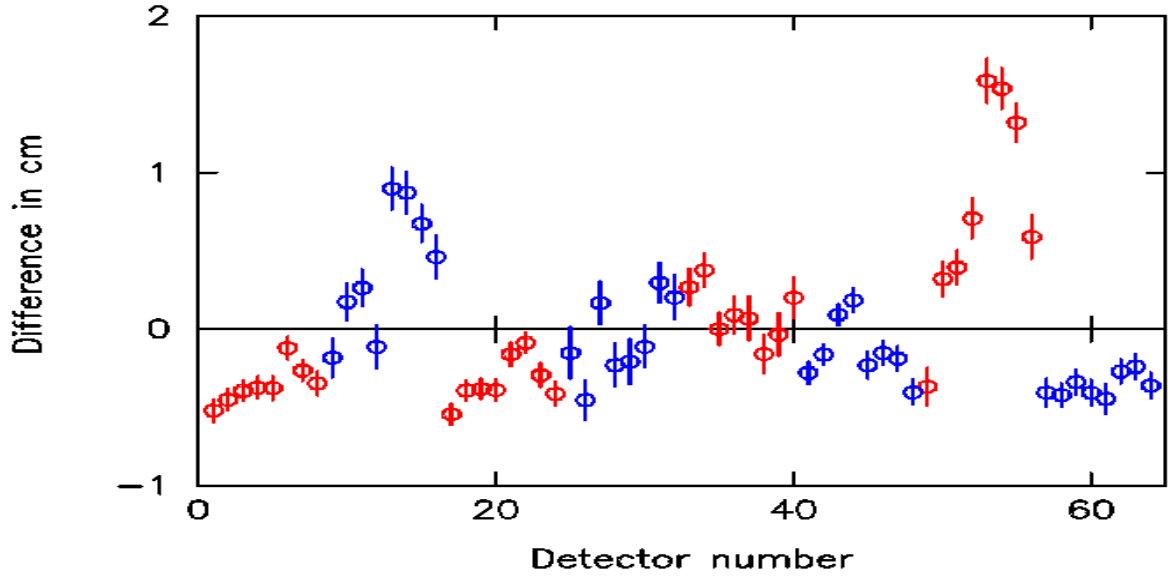


Figure 10a. Shows the difference in cm between values of $L_1$ obtained by the calibration procedure and a direct measurement. (calibration - direct measurement).

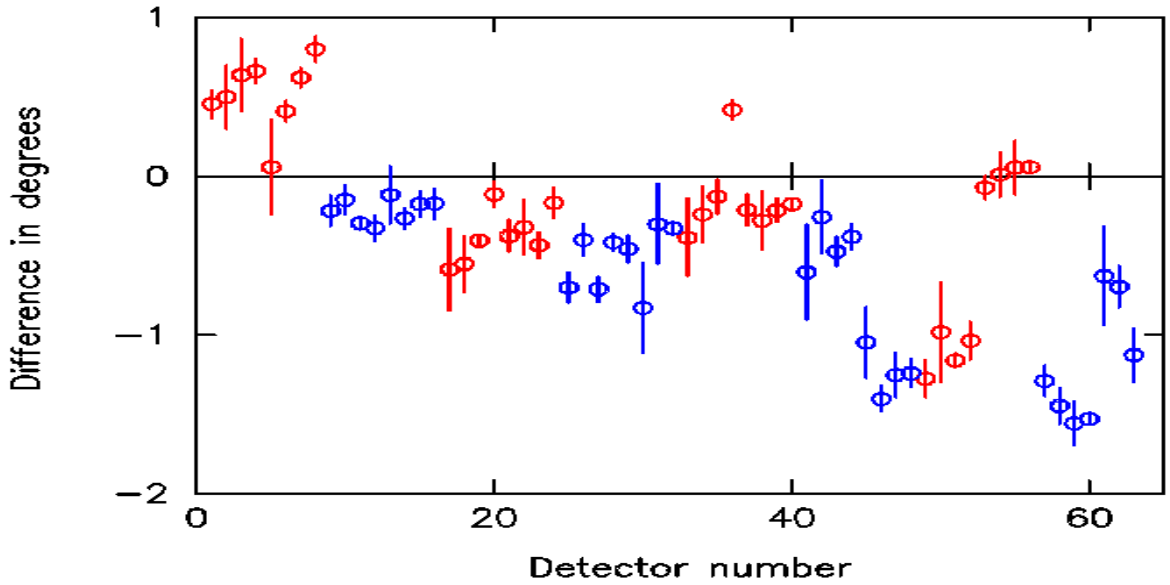


Figure 10b. The difference in degrees between the scattering angles measured using neutrons and a direct measurement (neutron measurement-direct measurement).

### 3f Determination of the Azimuthal Angle

For measurements on aligned samples (e.g. single crystals) it is necessary to exactly specify the position of each detector in three dimensions. The positions of the detector centres relative to the sample centre are specified most conveniently in spherical coordinates $(r,\theta,\phi)$. The coordinate system chosen is z along the beam direction and y vertical pointing upwards. By the right hand rule the x axis is horizontal and points to the left, looking along the beam from moderator to sample (fig. 11). The azimuthal angle $\phi$ is calculated from the directly measured values of $y_D$, the distance of the detector centre above or below the horizontal plane containing the beam centre, and the values of $L_1$ and $\theta$ obtained from the neutron calibrations given in sections 3c and 3d. The final instrument parameter table for forward scattering, containing the mean values of $L_0$, $L_1$, $E_1$, $t_0$, $\theta$ and $\phi$ for each detector is given in Appendix 4. This table is read by the analysis programs.

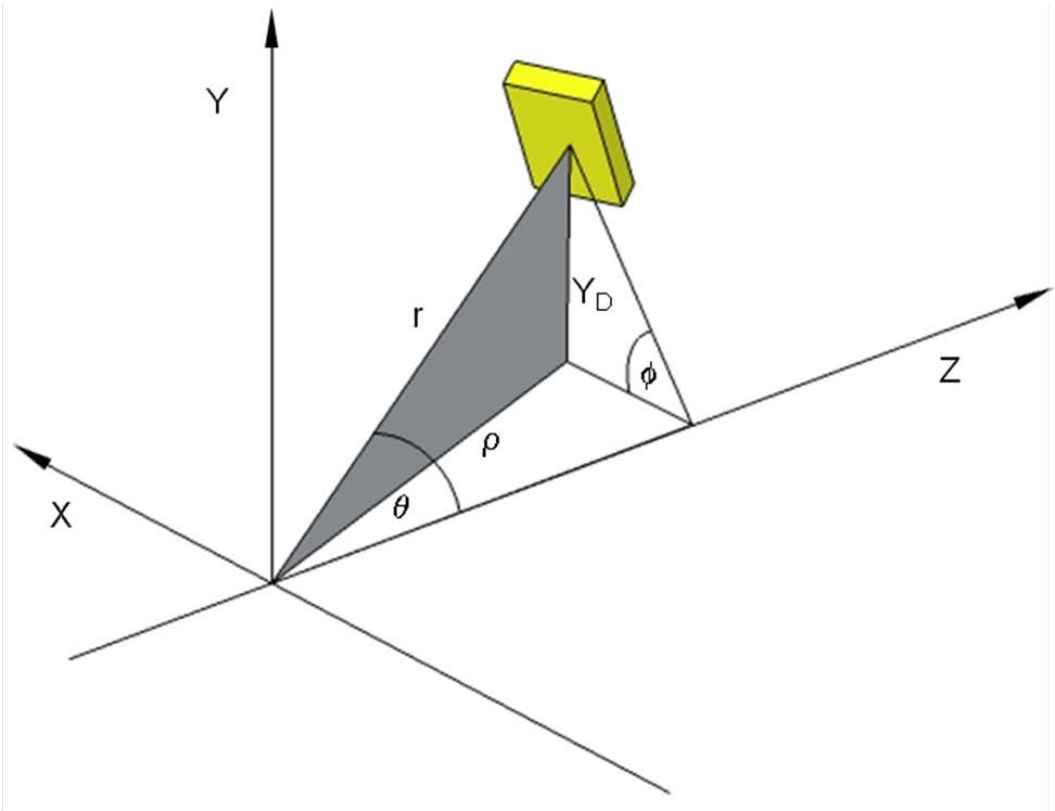


Figure 11. Coordinate system used to define the detector positions in three dimensions. The beam lies along the z axis. The y axis is vertical. $r = L_1$ is the distance from sample to detector. $\theta$ is the total scattering angle. $\phi$ is the azimuthal angle in the spherical coordinate system $(r,\theta,\phi)$

# 4. Determination of the Instrument Resolution

### 4a Pulse Width and Uncertainty in the Measurement of t

For energies >~1eV on pulsed sources, the pulse width (that is the duration in time of the pulse of neutrons of a given energy) is inversely proportional to the incident neutron velocity [22]. Hence it can be characterised in terms of an uncertainty $\Delta L_0$ in the incident flight path. The pulse width should be distinguished from the uncertainty $\Delta t$ in the value of $t$ assigned to the neutron, determined for example by the bin width chosen and by the limitations of the counting electronics.

The Gaussian fits to the resonance peaks shown in Figure 2 give a width in $t$ for each peak, in addition to the peak position. This width has components due to the intrinsic width of the absorption resonance, the uncertainty $\Delta t$ with which $t$ can be measured and the uncertainty $\Delta L_0$ in the incident flight path (or equivalently the pulse width in time). It is assumed that all distributions are Gaussian so that these widths add in quadrature. The fitted width in $t$ ($\sigma_{tot}$) is therefore given by

$$\sigma_{tot}^2 = \frac{{\Delta L_0}^2}{v_R^2} + {\Delta t_R}^2 + \Delta t^2 \qquad (5)$$

where

$$\Delta t_R = \frac{t_R}{2}\frac{\Delta E_R}{E_R} \qquad (6)$$

is the intrinsic width of the absorption line calculated using the values listed in table 1 . Calculated values of $v_R, \Delta t_R$ and the average of measured values of $\sigma_{tot}$ are given for the three peaks in table 3.

| $E_R$ (meV) | $v_R$ (m/sec) | $\Delta t_R$ (μsec) | $\sigma_{tot}$ (μsec) |
|---|---|---|---|
| 6672 | 35725 | 1.21 | 1.38 ± 0.02 |
| 20874 | 63190 | 0.38 | 0.62 ± 0.01 |
| 36684 | 83768 | 0.24 | 0.51 ± 0.01 |

**Table 3.** $E_R$ is the calculated energy at the centre of the uranium absorption line. $v_R$ is the corresponding neutron velocity. $\Delta t_R$ is the calculated width in $t$ of the absorption line. $\sigma_{tot}$ is the average over the 64 YAP detectors of the fitted width in $t$. The quoted error is the standard error in the mean.

It follows from eq. (5) that from a least squares fit of $\sigma_{tot}^2$ against $1/v_R^{\ 2}$ the value of $\Delta t$ can be determined from the intercept and $\Delta L_0$ from the gradient. The values of $\Delta L_0$ obtained for the 64 detectors by this procedure are shown in Figure 12a. The values of $\Delta t$ obtained are shown in Figure 12b.

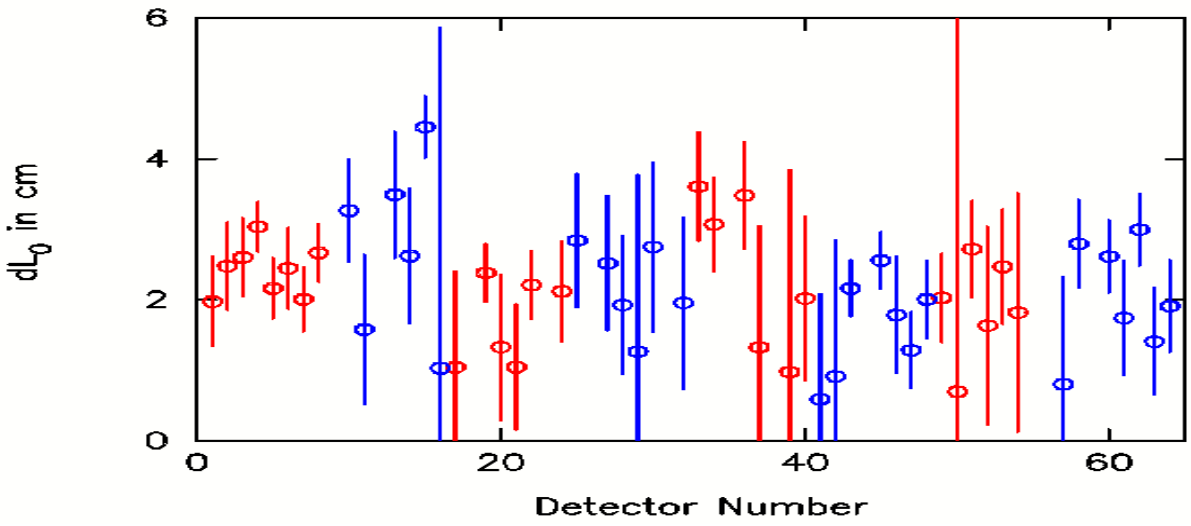


Figure 12a. Values of $\Delta L_0$ obtained as a function of detector number. The mean value is 2.4 ± 0.1 cm.

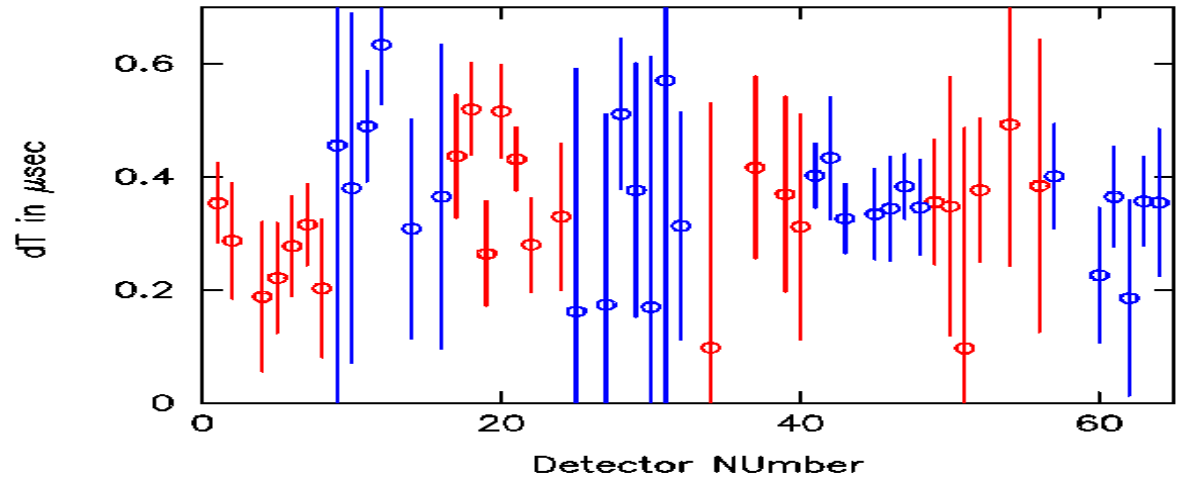


Figure 12b. Values of $\Delta t$ obtained from the calibration. The mean value was 0.37 ± 0.02

The mean value $\Delta t$ = 0.37 ± 0.02 μsec is determined essentially by the bin width of 0.5 μsec in the time of flight spectra. The mean value of $\Delta L_0$ =2.4 ± 0.1 cm agrees well with the value (2.0 ± 0.2 cm) derived previously by measuring the transmission of a U foil [11]. For an incident energy of 1 eV the FWHM of the pulse width given by calculations performed during

the design phase of the moderators of ISIS [22] is ~1 μsec. The calibrated value of $\Delta L_0$ gives a value of ~1.5 μsec at 1 eV. Given the assumptions in the analysis (in particular that the pulse shape is Gaussian), the agreement between measurement and calculation is satisfactory.

**4b Uncertainty in $L_1$**

The uncertainty in $L_1$ is due to the different possible positions that neutrons can be scattered from the sample, due to the finite beam and sample size and the different possible positions where they can be incident on the detector, due to the finite detector size. This was calculated by a Monte Carlo simulation using the known detector size (8cm x 2.5cm) ,taking a circular beam with a mean diameter of 4 cm and assuming a slab sample perpendicular to and covering the incident beam. The positions of the detectors in three dimensions, determined in section 3, were used to define the geometry of the instrument. The calculated values of $\Delta L_1$ (which was taken as the r.m.s. deviation from the mean of the events in the simulation) are shown in Figure 13.

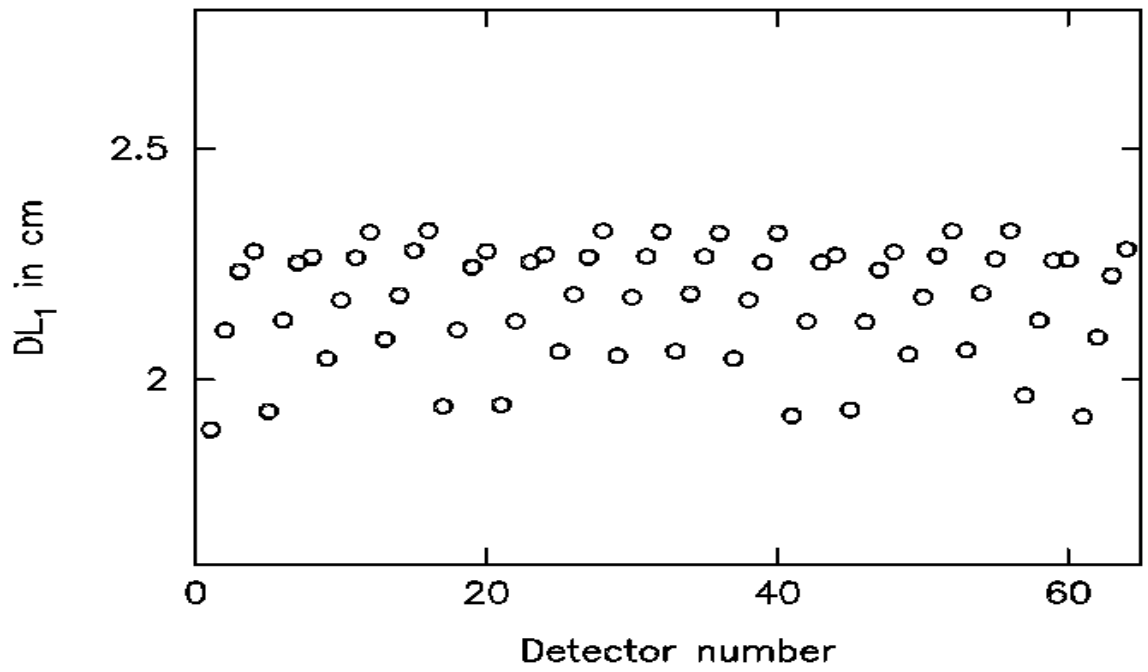


Figure 13. Values of $\Delta L_1$ calculated as a function of detector number. The mean value is 2.3 ± 0.2 cm. The values shown in Figure 13 are listed in the table used to define the instrument resolution in Appendix 5.

**4c Uncertainty in $E_1$**

The uncertainty in the final energy $\Delta E_1$ is determined from the calibration run with the Pb sample. Data from a single YAP detector is shown in Figure 6, together with the fit of a Voigt function. The width of the peak is determined by: (i) by the intrinsic width due to the distribution of momenta of lead atoms in the sample - this is shown as the blue dotted line, (ii) the values of $\Delta L_0, \Delta t$ and $\Delta L_1$ determined in sections 4a and 4b and (iii) the distribution of scattering angles $\Delta\theta$, determined in section 4d. However the energy resolution is the dominant contribution to the width with a lead sample (see Figure 19e).

It is assumed that all contributions to the width other than that from the energy resolution give a Gaussian distribution in $t$. The quality of the fits shown in Figures 4 and 6 shows that this assumption introduces no noticeable inaccuracies. Thus these contributions can be subtracted in quadrature from the fitted Gaussian component of the Voigt function to determine the Gaussian and Lorentzian components of the energy resolution function. The widths extracted from the fits were converted to an equivalent width in energy using eq. (6). The fitted values of the Lorentzian component $\Delta E_{1L}$ and the Gaussian component $\Delta E_{1G}$ obtained from fitting are shown in Figures 14a and 14b for the 64 YAP detectors.

The mean value of $\Delta E_{1L}$ was 24 ± 1 meV. The mean value of $\Delta E_{1G}$ was 73 ± 0.5 meV. The errors quoted are the standard error in the mean over 64 detectors. The individual values of $\Delta E_{1L}$ and $\Delta E_{1G}$ shown in Figures 14a and 14b are stored in a resolution file (Appendix 5) which can be read by the analysis programs.

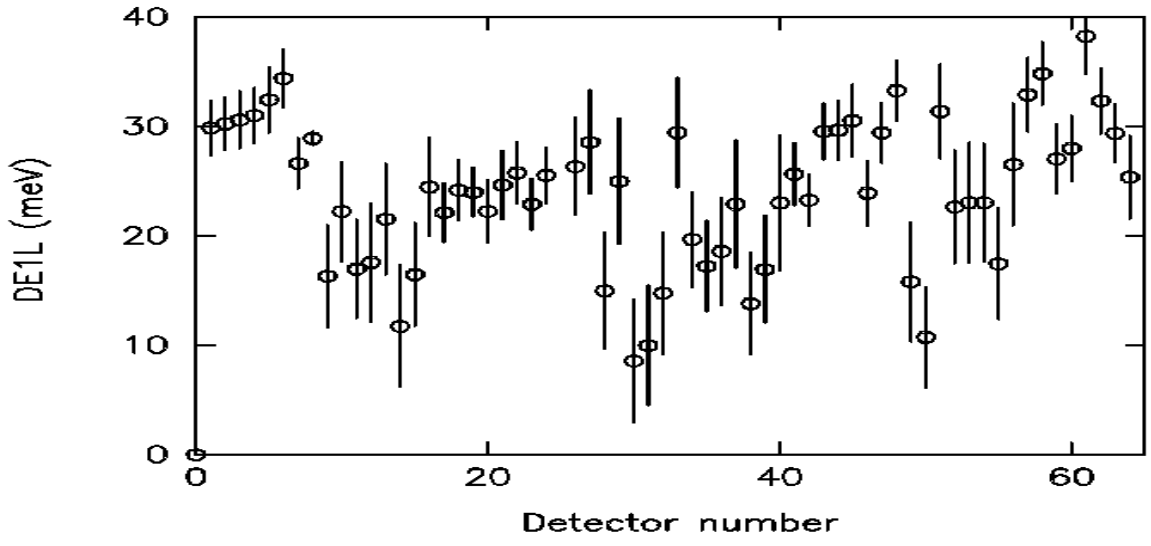


Figure 14a. Values of the Lorentzian HWHM of the energy resolution function. The mean is 24 ± 1 meV.

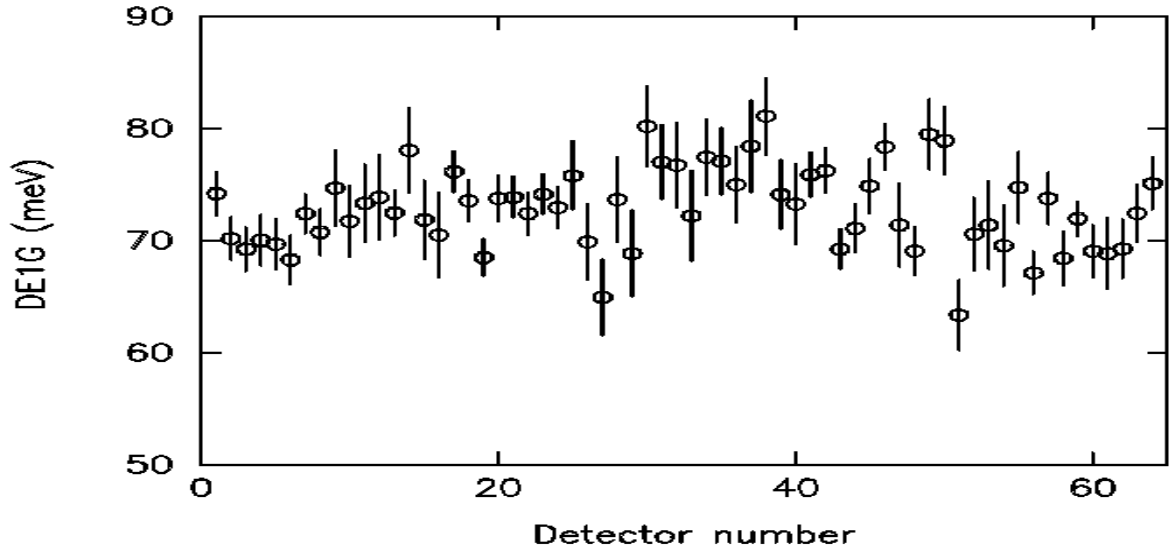


Figure 14b. Values of the Gaussian SD of the energy resolution function. The mean is 73 ± 0.5 meV

**4d Uncertainty in Angle**

The uncertainty in scattering angle was determined by measuring the widths of Bragg peaks obtained from the standard Pb calibration sample (see Figure 8). The width of the peaks at forward scattering angles is totally dominated by the angular resolution of the detectors. Hence the range of neutron wavelengths in the peak is given by eq. (4) as

$$\Delta\lambda = 2d\cos\theta\Delta\theta \qquad (7)$$

It follows that

$$\frac{\Delta\lambda}{\lambda} = \frac{\Delta t_\theta}{t} = \frac{\Delta\theta}{\tan\theta} \qquad (8)$$

where $\Delta t_\theta$ is the fitted Gaussian standard deviation of the peaks in $t$. The resolution of the detector can be defined in terms of an effective width DW, defined as

$$DW = L_1\Delta\theta \qquad (9)$$

Gaussian fits were made in t to the 3 highest order Bragg peaks for each spectrum and the values of $\Delta t_\theta / t$ were determined for each peak. DW was calculated as the mean of the 3

values obtained from the fitted values of $\Delta t_\theta / t$. Figure 15a shows calibrated values of DW for all 64 detectors as the black circles. The error bars are the standard error in the mean of DW values calculated from the three fitted values of $\Delta t_\theta / t$. The figure also shows as red crosses the values of DW calculated by Monte Carlo integration using the measured instrument geometry. Figure 15b shows the differences between the calibrated value of DW and the calculated values. It can be seen that the qualitative agreement between calibration and calculation is good. The systematic variation in DW within a single column of groups of 4 detectors seen in the calibration is reproduced in the calculation. This variation is due to the fact that the detectors are in an almost vertical column and do not lie on the Debye-Scherrer cone. As the z value of a detector increases the deviation from the Debye-Scherrer cone increases, hence the angular resolution worsens. The differences between calibration and calculation are probably due to the difficulty of precisely defining the instrument geometry in the calculation. For example it is assumed that the plane of the scintillation glass is perpendicular to the line joining the sample and detector centres. Any misalignment of the detectors will lead to an error in the calculated value of DW, although it will not affect the accuracy of the calibration.

It can be seen by examination of Figure 15b and Figure 9 that the largest deviations between calculation and calibration occur at the lowest scattering angles, where deviations of the detector geometry from the Debye-Scherrer cone produce the largest effects. Again this suggests that the difficulties of defining the exact detector geometry are responsible for the differences between calculation and measurement seen in Figure 15b.

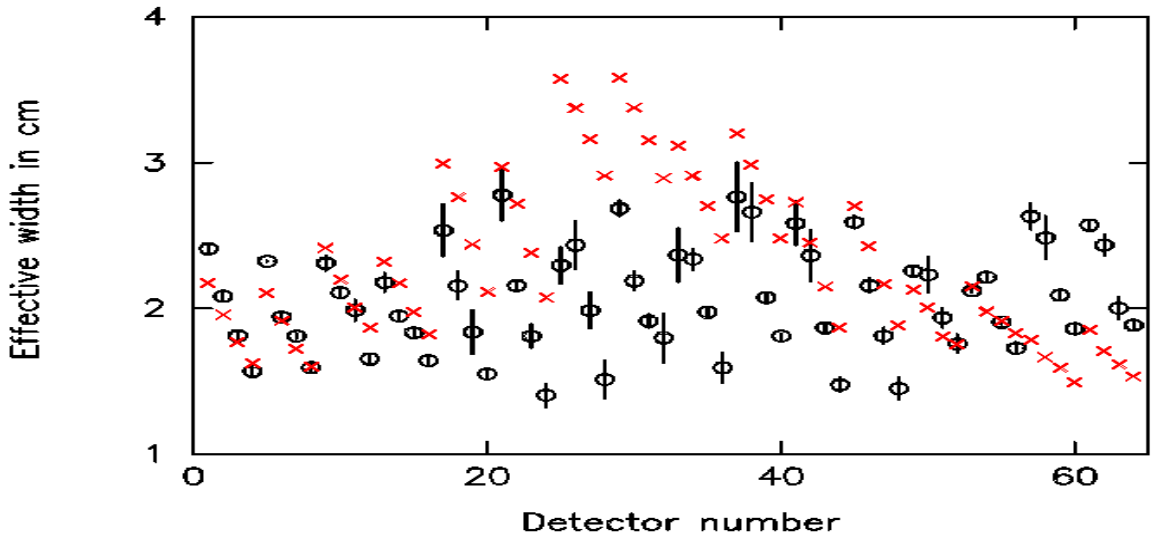


Figure 15a. Values of DW determined by the calibration procedure described are shown as the black circles, with errors. Those calculated by Monte Carlo integration using the measured instrument geometry are shown as red crosses.

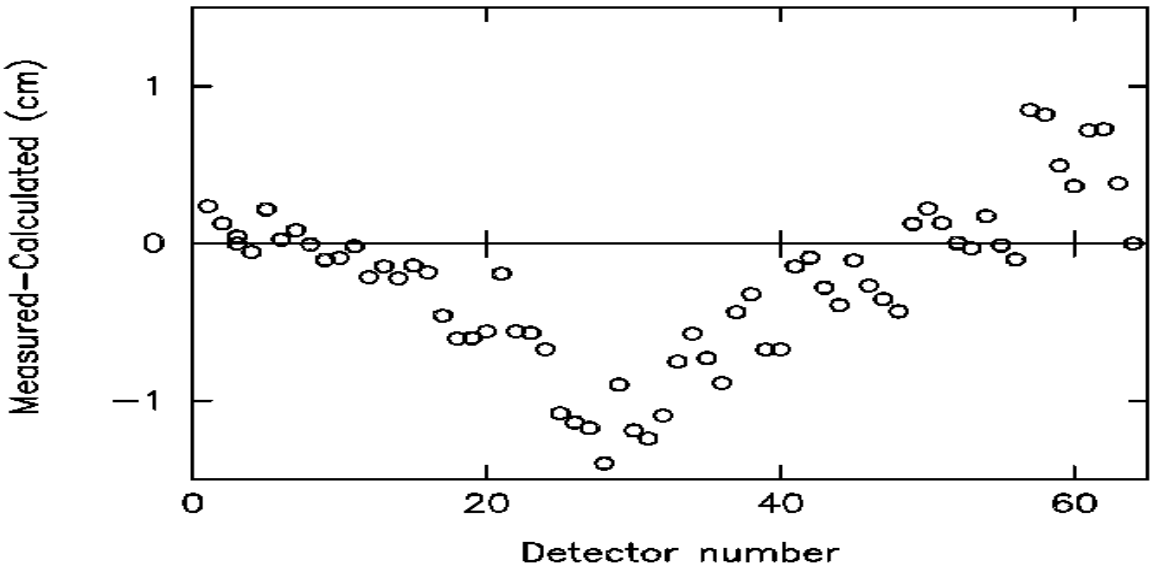


Figure 15b. Difference between calculated and calibrated values of DW in cm. The largest differences occur at the lowest scattering angles.

The resolution components determined by the calibration procedures given in this section are stored in a file which is read by the standard VESUVIO data analysis programs. This file is given in Appendix 5.

## 5. Calibration of Back-scattering detectors

The methods used to calibrate the back scattering detectors are very similar to those described in sections 3 and 4 for the forward scattering detectors. However there are some differences due to the different methods for neutron detection used at backward and forward angles. Many of the procedures in this section have already been described in ref [11]. The values of $L_0$ and $\Delta L_0$ are the same for both forward and back-scattering. Hence the values of these quantities derived in sections 3a and 4a are used for all detectors. The procedure for defining the final energy and energy resolution has already been described in sections 3b and 4c.

### 5a Determination of the Mean Values of $L_1$ and $t_0$

The values of $L_1$ and $t_0$ are determined by a calibration run with a thin uranium foil in the incident beam and a lead sample. The spectra in the $^6$Li back-scattering detectors contain absorption lines due to neutrons in the incident beam being absorbed by the uranium resonances. A typical spectrum is shown in Figure 16

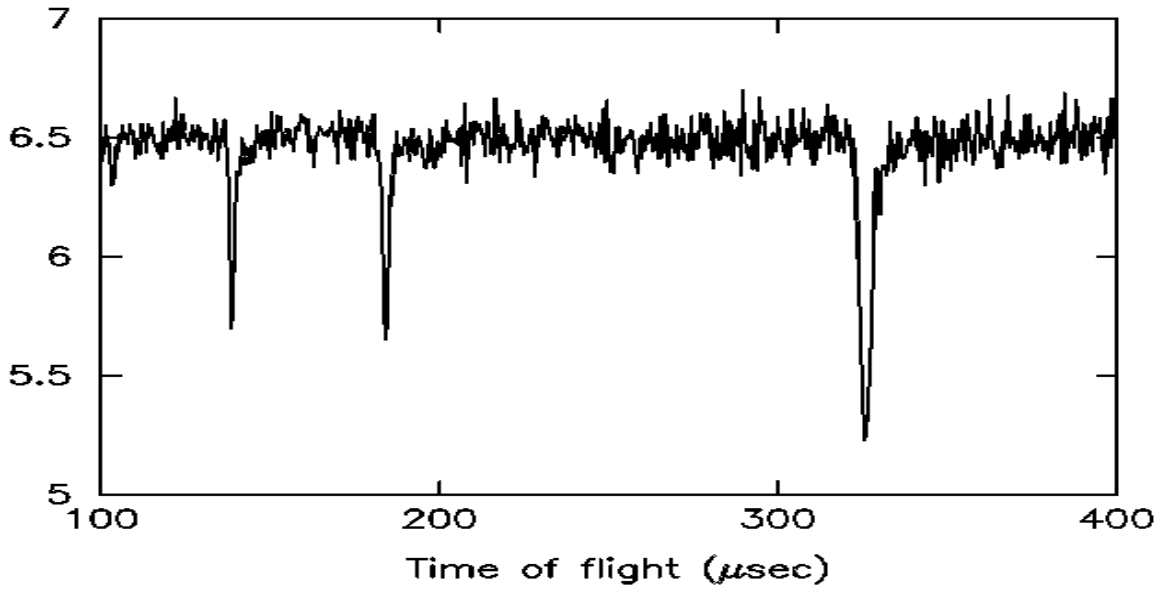


Figure 16. A typical spectrum from one of the 132 back-scattering detectors, obtained by scattering from the lead calibration sample with a uranium foil in the incident beam. The data is divided by scattering from a lead calibration with no uranium foil to remove the spectrum shape.

The absorption lines are fitted to Gaussians and the values of the time delay $t_0$ and the total flight path $L = L_0 + L_1$ is obtained from the fitted peak positions in time of flight. (The method is described in ref [11] and is almost identical to that used in section 3a to determine $t_0$ and $L_0$). The value of $L_1$ is determined using the value of $L_0$ obtained in section 3a. The values of $L_1$ are shown for the 132 back-scattering detectors in Figure 17a and those for $t_0$ in Figure 17b. Also shown in Figure 17a as the red circles are the values of $L_1$ obtained using the lead calibration run with no uranium foil in the incident beam and the procedure described in section 3c. The two procedures are in good agreement. The values of $L_1$ obtained from the lead calibration are preferred as they have better statistical accuracy. They are listed in Appendix 6 for each detector.

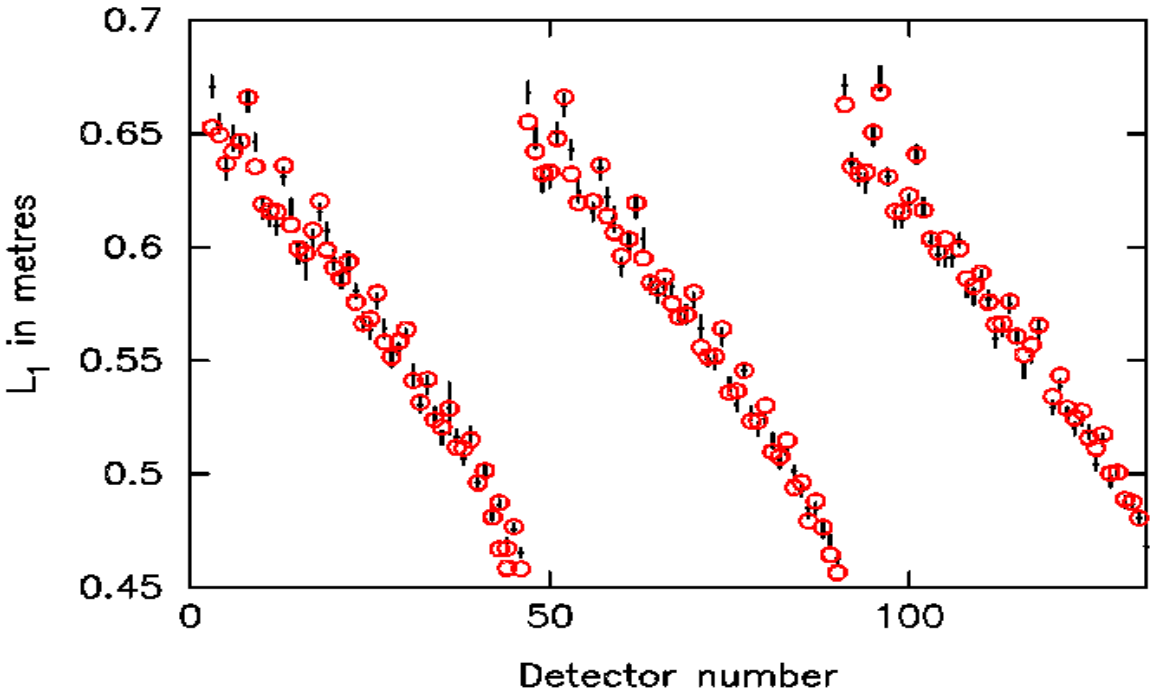


Figure 17a. Shows calibrated values of $L_1$ for the 132 back-scattering detectors The points with error bars were obtained using the lead calibration sample with a uranium foil in the incident beam. The red circles were obtained by fitting the positions of the lead peaks obtained from the differenced data, with no uranium foil in the incident beam.

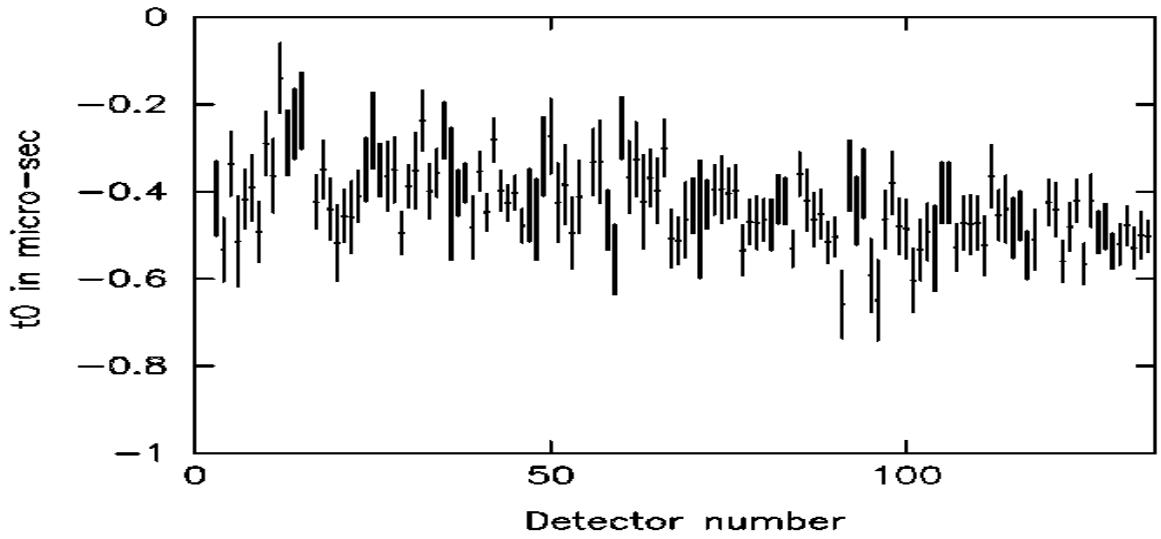


Figure 17b. Shows calibrated values of $t_0$ for the 132 back-scattering detectors.

**5b Determination of the resolution components Δt, $\Delta L_1$**

The values of $\Delta t$, the uncertainty in the measurement of $t$, and $\Delta L$, the uncertainty in the total flight path are determined from the fitted widths of the absorption lines, illustrated

in Figure 16. The procedure used is described in reference [11] and is very similar to that followed in section 4a. Figures 18a and 18b shows the values obtained for $\Delta L$ and $\Delta t$ in spectra 3-135.

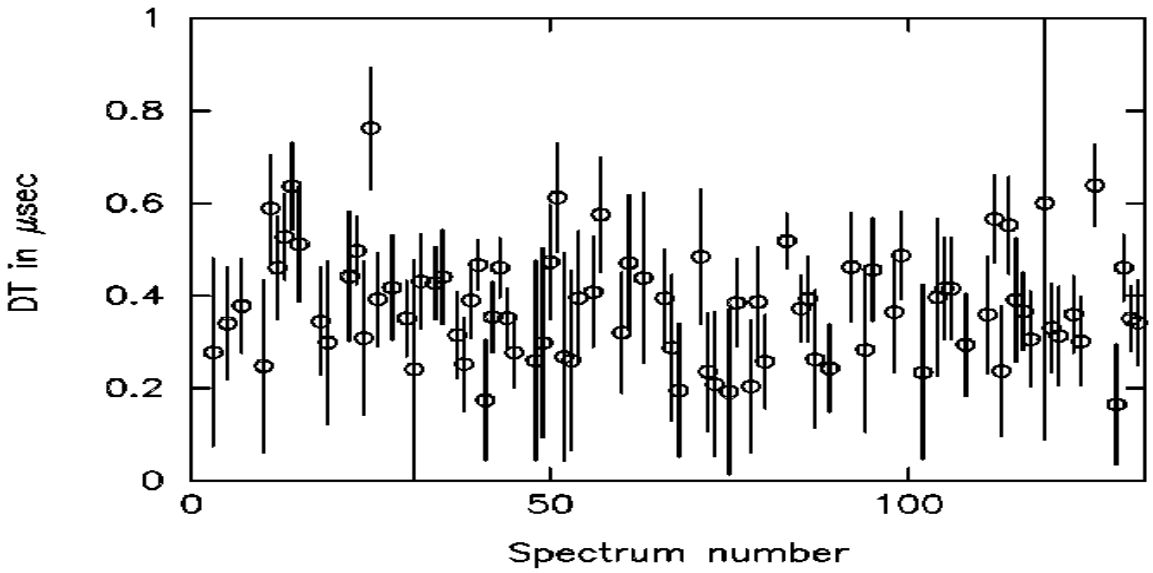


FIGURE 18a. Values of $\Delta t$ in microsec for the 132 back-scattering detectors.

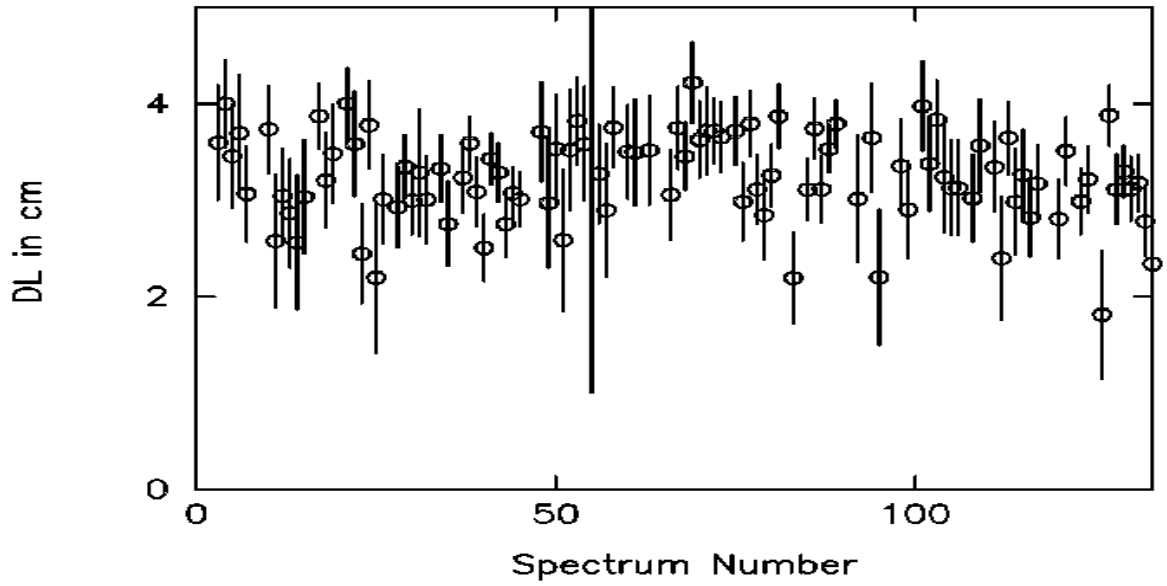


FIGURE 18b. Values of $\Delta L$ in cm for the 132 $^{6}$Li doped back-scattering detectors.

From the value of $\Delta L_0$ = 2.4 cm, calibrated in section 4a, the uncertainty in the final flight path is determined as

$$\Delta L_1 = \left[\Delta L^2 - \Delta L_0{}^2\right]^{1/2} \qquad (10)$$

Eq. (10) implicitly assumes that $L_0$ and $L_1$ have a Gaussian distribution about their mean value and that there is no correlation between these parameters. Table 4 lists the average values of $t_0$, $\Delta t$, $\Delta L_1$ and $E_1$ over the three banks of 44 detectors. Also listed for comparison are the values obtained for the YAP detectors at forward angles in sections 3 and 4.

| **Detector bank** | **$t_0$** | **$\Delta t$** | **$\Delta L_1$** | **$E_1$** |
|---|---|---|---|---|
| S3-S46 ( $^6$Li) | -0.39 ± 0.01 | 0.42 ± 0.02 | 2.2 ± 0.1 | 4897.1 ± 0.7 |
| S47-S90 ( $^6$Li) | -0.44 ± 0.01 | 0.38 ± 0.02 | 2.5 ± 0.1 | 4897.5 ± 0.7 |
| S91-S132 ( $^6$Li) | -0.49 ± 0.01 | 0.40 ± 0.02 | 2.1 ± 0.1 | 4895.6 ± 0.8 |
| S135-S198 (YAP) | -0.40 ± 0.02 | 0.37 ± 0.02 | 2.2 ± 0.2 | 4897.0 |

**Table 4** gives the calibrated values of various parameters for the three back-scattering banks and the 64 YAP detectors.

## 6. Resolution for different masses

The VESUVIO spectrometer measures the momentum distribution of atoms. The momentum of the atoms is conventionally given in terms of the wave vector $k$ measured in Å$^{-1}$. (This can be converted to momentum using the de Broglie relation $p = \hbar k$ .) Hence the resolution components are also given in Å$^{-1}$. Values of these components for the best current resolution of VESUVIO in momentum space are given for hydrogen in Figure 19a, deuterium in Figure 19b, lithium in Figure 19c , oxygen in Figure 19d and lead in Figure 19e. The resolution for $^4$He at back-scattering is given in Figure 19f. All resolution components are assumed to be Gaussian, except for the energy resolution function which is a convolution of a Lorentzian and a Gaussian.

It can be seen that in all cases the resolution function is dominated by the uncertainty with which the final energy and the scattering angle are known. This implies that any inaccuracies in the calibration procedure for the mean and distribution of values of $L_1, L_0$ and $t$ (in particular that the distributions are Gaussian) should have negligible effect. That this is so is also clear from the quality of the fits obtained in Figures 4 and 6. Generally the energy resolution is dominant, but for measurements of hydrogen (which is the main application of VESUVIO) the angular resolution dominates.

The resolution for H measurements is typically ~25% of the intrinsic width due to the zero point motion of protons. For D it is ~20%, for Li ~30% , for O ~25%. Hence in these

cases the shape of the momentum distribution can be measured with reasonable accuracy. For scattering from heavier elements the resolution becomes progressively worse. Liquid and solid $^4$He and $^3$He are a special case due to their extremely narrow momentum distributions. In these cases the resolution is at present too poor to measure peak shapes and only mean kinetic energies of atoms can be determined.

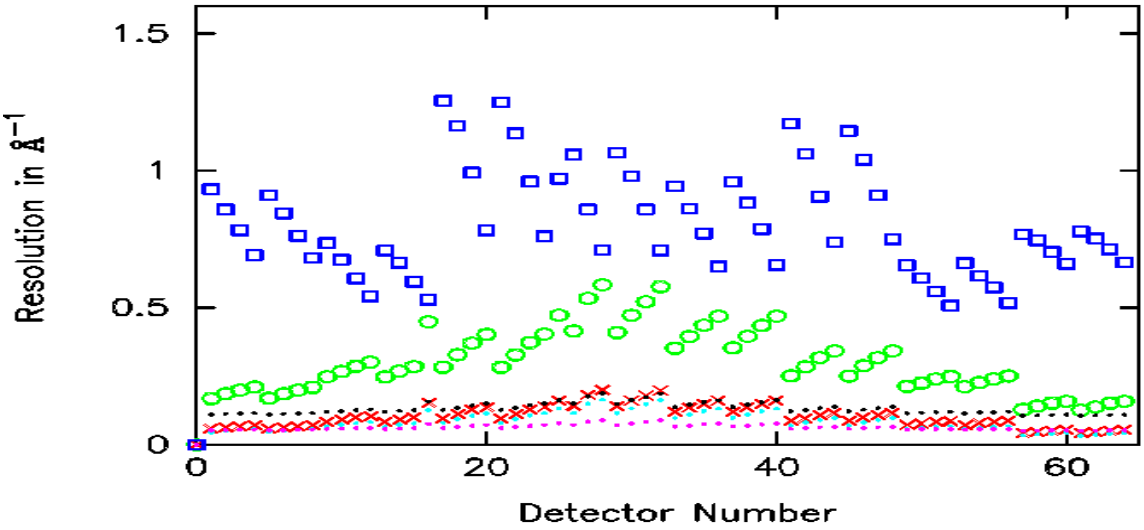


Figure 19a. The resolution for scattering from H in the forward scattering YAP detectors. Typical H peak widths are in the range 3-5 Å$^{-1}$.

□ Angular resolution, o Gaussian component of energy resolution, x Lorentzian component of energy resolution, • Component due to uncertainty in $L_0$, • Component due to uncertainty in $L_1$ , • Component due to uncertainty in t.

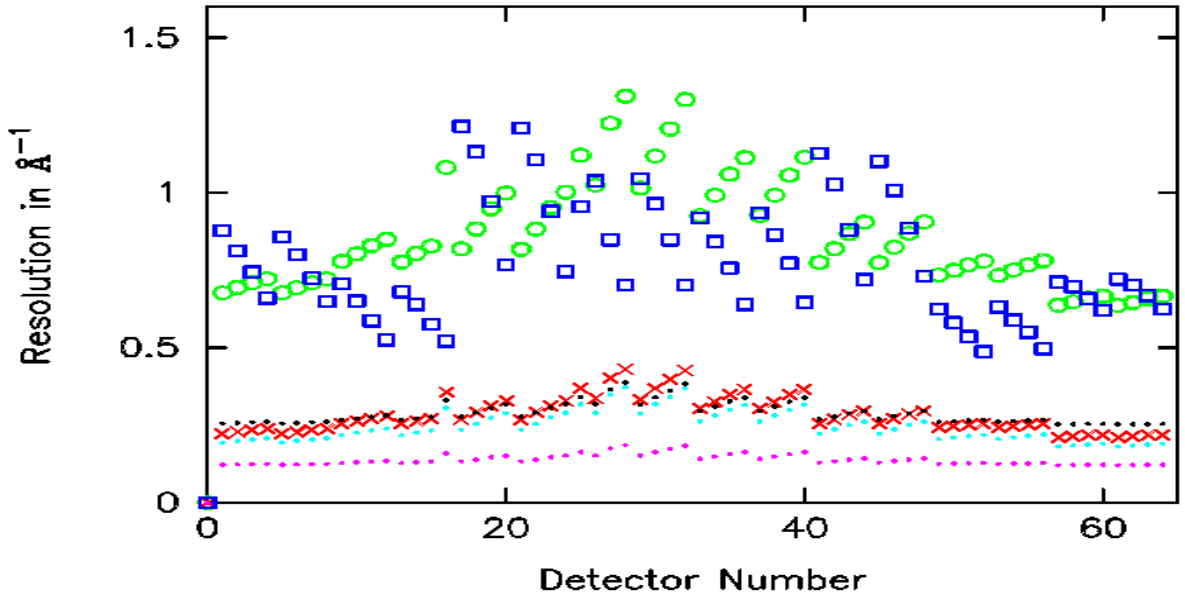


Figure 19b. The resolution for scattering from D in the forward scattering bank. Typical D peak widths are in the range 4-6 Å$^{-1}$.

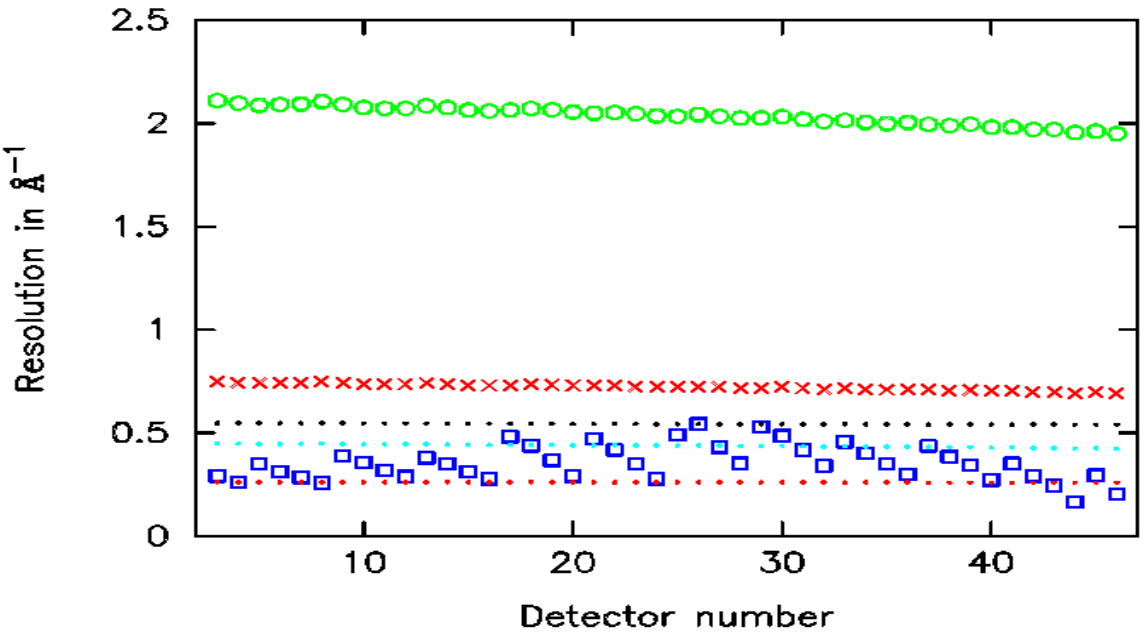


Figure 19c. Resolution for $^{7}$Li at back scattering with the double difference technique. Typical Li peak widths are ~4-7 Å$^{-1}$.

□ Angular resolution, o Gaussian component of energy resolution, x Lorentzian component of energy resolution, • Component due to uncertainty in $L_0$, • Component due to uncertainty in $L_1$ , • Component due to uncertainty in t.

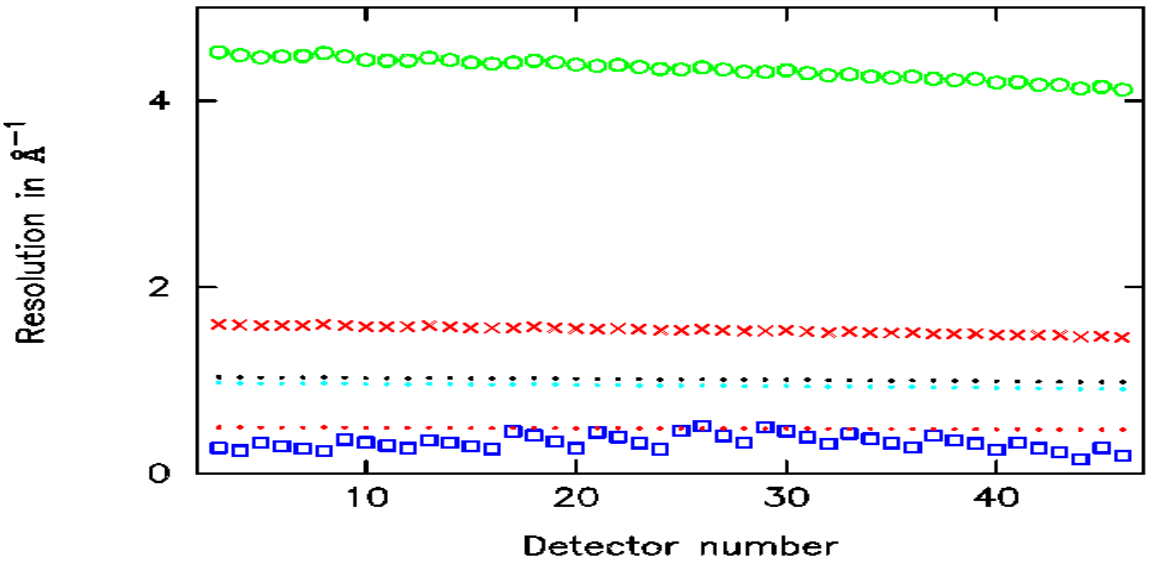


Figure 19d. Resolution for O at back-scattering with the double difference method.. Typical O peak widths are ~10-15 Å$^{-1}$.

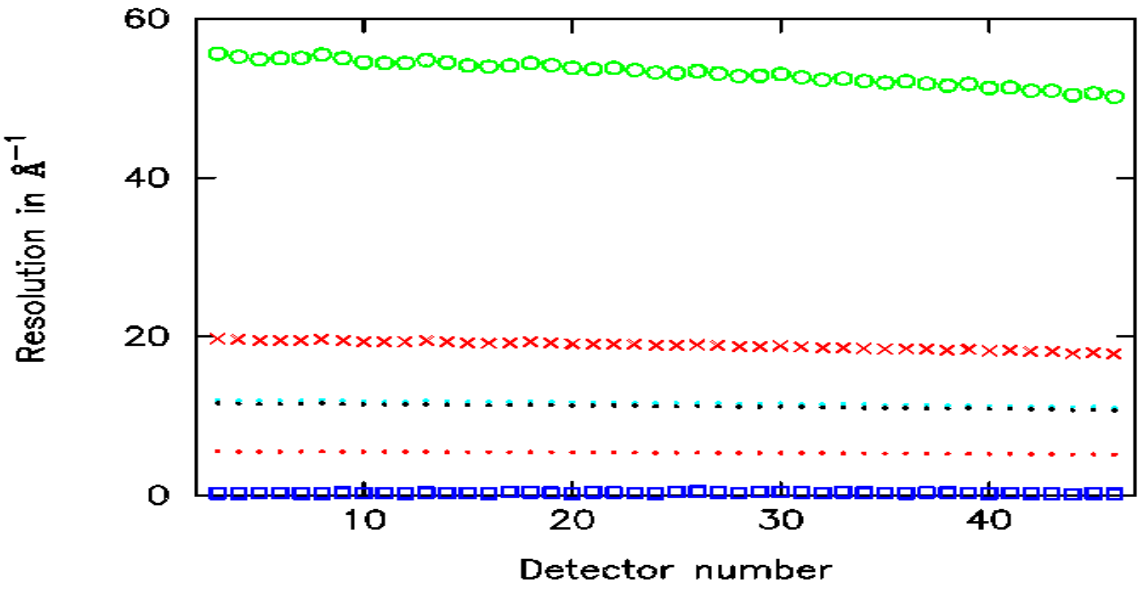


Figure 19e. Resolution for Pb at back-scattering with the double difference method. The width of the Pb peak at 300K is 35.3 Å$^{-1}$.

□ Angular resolution, o Gaussian component of energy resolution, x Lorentzian component of energy resolution, • Component due to uncertainty in $L_0$, • Component due to uncertainty in $L_1$ , • Component due to uncertainty in t.

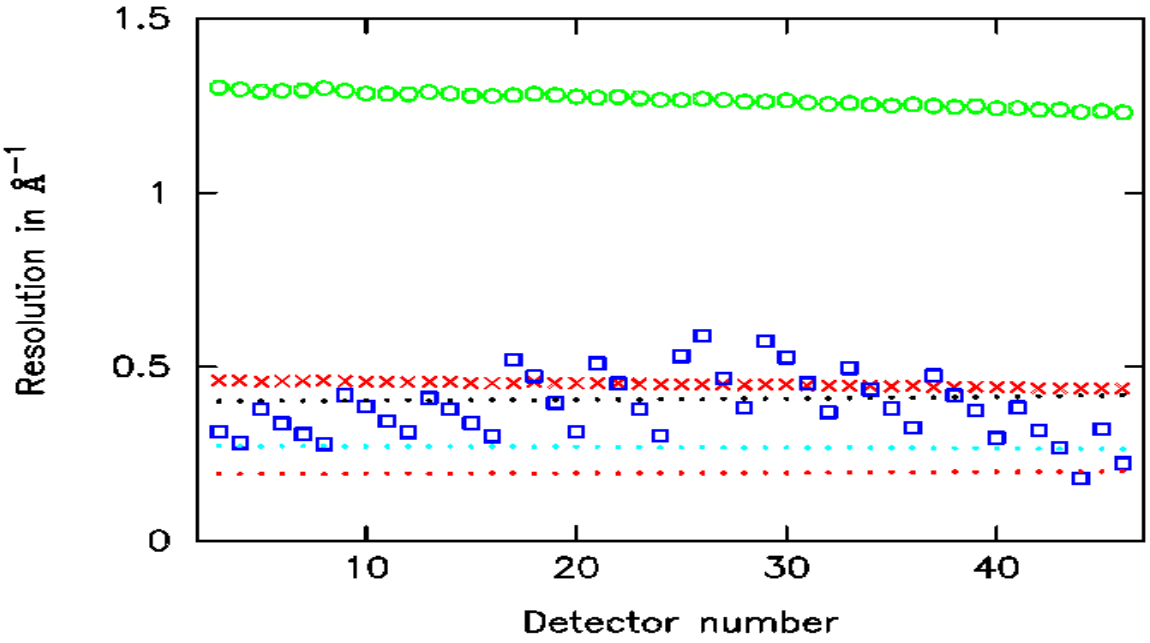


Figure 19f. Resolution for He4 at back scattering with the double difference method. Typical peak widths in liquid and solid He4 are ~1 Å$^{-1}$.

## 7. Conclusions

The procedure used to calibrate the VESUVIO spectrometer at ISIS has been described. The results of the calibrations suggest a number of improvements which could be made to the instrument:

(1) The dominant contribution to the resolution for measurement of protons is the angular resolution of the instrument and as most of the applications of the instrument involve measurements on protons, efforts should be made to improve this by, for example, moving the detectors further away (although this would lead to a drop in count rate without more detectors).

(2) A preferable geometry for the forward scattering bank would be to place the detectors on Debye-Scherrer cones about the beam axis. Figures 15a and 19a show that this would improve the resolution of some detectors by a factor of ~2. This geometry has the additional advantage that the correction currently applied for the gamma background from the moving analyser foils would be almost negligible compared with its present ~5% level [20].

(3) The resolution at back-scattering could be much improved by replacing the $^6$Li neutron detectors with YAP detectors. With a uranium foil at room temperature on the detectors and a uranium foil cooled to ~40K in the differencing device the energy resolution for studies of $^4$He and $^3$He would be comparable with existing chopper spectrometers, but with much higher momentum transfers and hence significantly reduced final state broadening (see [19] and references therein). This would open a whole new range of applications of the instrument to the study of quantum fluids and solids. The resolutions which could be obtained are listed in table 5.

| $E_R$ (meV) | $\Delta E_R$ (meV) | $\Delta y_R$ (Å$^{-1}$) | Q ((Å$^{-1}$) |
|---|---|---|---|
| 6672 | 73 | 0.82 | 137 |
| 20874 | 127 | 0.82 | 243 |
| 36681 | 195 | 0.94 | 323 |

**Table 5.** $E_R$ is the energy of the uranium resonance. $\Delta E_R$ is the FWHM of the energy resolution, $\Delta y_R$ is the FWHM of the resolution in momentum space for $^4$He, Q is the momentum transfer. The FWHM of the intrinsic width of the $^4$He momentum distribution is ~2.1 Å$^{-1}$.

# Appendix 1. Programs and data used to determine mean instrument parameters

Unless otherwise specified, all programs referred to are stored on the ISIS VMS system in

EVS$DISK0:[EVSMGR.CALIB]

### A1a Determination of Final Neutron Energy

The data in Figure 4 was a sum of Pb calibration runs performed between Sept 2008 and Feb 2009 (Runs 14067-71, 14043-50, 13895-13901, 13369-72 and 13352-55). The total μamphrs was 24000. The time of flight data were corrected for gamma background and multiple scattering and are stored in the GENIE files [.TOTAL]PBMS.1… PBMS.64. The fits to each detector were performed using the routine PBFIT.COM and STORED in PBMS.DAT. The final neutron energy was determined using the routine PBPLOT.FOR. The gold foil absorption shown in Figure 5 was calculated using the program EVS$DISK:[EVSMGR.FOILS]TRANS.FOR

### A1b Determination of Incident Flight Path

The run with the U foil at the sample position was number 14025 (45.6 μamphrs). This was divided by Pb run 12570 (2799 μamphrs) to remove the incident spectrum shape. The GENIE command file TRANSFITYAP.COM was used to fit Gaussians to the peaks. This produces files: [.DATA]U7_14025.DAT, [.DATA]U21_14025.DAT, [.DATA]U37_14025.DAT containing the positions with statistical error of the Gaussian fit in time of flight for each detector and the standard deviation with error of the Gaussian fitted. These files can be examined using PLOTU.FOR. Figures 3a and 3b and the mean values were obtained by running the program LTCALIB.FOR.

### A1c Determination of Final Flight Path

The data used to determine the final flight path was a sum of the same Pb calibration runs used in section A1a. The positions and widths of the peaks in time of flight were determined using the GENIE command file PBFIT.COM. This fits a convolution of a Lorentzian and a Gaussian to the peak (see Figure 6) and produces a file containing the intensities, positions, Gaussian and Lorentzian widths in time of flight and the reduced chi-

square of the fit. This was stored as PBMS.DAT. The final flight paths are calculated from this data file using the routine L1CAL.FOR, which outputs a file L1.DAT.

**A1d Determination of Total Scattering Angle**

The data used was a ratio of the PB run 14043 (900 μamphrs) and vanadium run 12573 (2970 μamphrs). The ratio of the time of flight spectra was calculated for each detector using the command file PBV.COM. The positions of the peaks were determined using the cursor in GENIE and the file [.DATA] PB14043.DAT was created. Figure 9 was produced by running the program ANGLE.FOR with PB14043.DAT as input.

**A1e Comparison with Direct Measurement**

The Detector positions determined by direct measurement are stored in [.YAP]DETPOS.DAT and contain the detector positions in cylindrical coordinates

| | $\rho$ | $\varphi$ | $y_D$ | |
|---|---|---|---|---|
| 1 | 0.4467000 | -59.60000 | 0.3359000 | |
| 2 | 0.4758000 | -59.70000 | 0.2604000 | etc. |

DETPOS.DAT was created from the original DETPOSMARK.DAT file by the program DETPOS.FOR.

$y_D$ is the distance of the detector centre in metres above or below the horizontal plane containing the beam centre and $\rho$ is the sample-detector distance in the horizontal plane (figure 11). The values in this table are used to calculate the total scattering angle $\theta$ via the program [.YAP]THCALC.FOR, which outputs a file THCALC.DAT. The final flight path is calculated using [.YAP]L1CALC.FOR which outputs a file L1CALC.DAT.

**A1f Determination of the Azimuthal Angle**

The program [.YAP]PARFILE.FOR was used to calculate the azimuthal angle $\phi$ in the coordinate system of section 3f. The input was the calibrated values of $\theta$ and $L_1$ and the values of $y_D$ in [.YAP]DETPOS.DAT. The program creates the file listed in Appendix 3.

# Appendix 2. Determination of the instrument resolution

### A2a $L_0$, t Resolution Calibration.

The uncertainties in $L_0$ and $t$ are determined using the program L0RES.FOR, with the files produced in section A1b as input. The output files are L0WID.DAT, TWID.DAT .

### A2b $L_1$ Resolution Calibration

The uncertainty in $L_1$ is determined by Monte Carlo calculation using [.YAP]ANGRESYAP2.FOR . This outputs a file DL1.DAT containing the uncertainty in $L_1$ for each detector.

### A2c Energy Resolution Calibration

The data used is the same as that used section A1c (PBMS.DAT). The routine PBPLOTFIGS.FOR produces output files E1.DAT, DEL.DAT and DEG.DAT.

### A2d Calculation of Angular Resolution of Detectors

The data used was that created in section A1c. A file [.YAP]DTOVERT.DAT was created by fitting Pb peaks in time of flight. Each peak was fitted separately using [.YAP]GFIT.FOR. The effective widths DW of the detectors were determined from the fitted Bragg peak widths using [.YAP]DL1CALC.FOR. This produces a file DL1CALC.DAT containing the effective widths of the detectors as a function of detector number.

The Monte Carlo calculations of DW were made using [.YAP]ANGRESYAP2.FOR. This outputs a file EW.DAT which contains the effective width of the detector.

### A2e Production of Resolution File

The program [.YAP]RPCREATE reads the output files by the programs in sections A2a-d and creates a file containing the resolution components for each detector.

## Appendix 3. Calibration of Back Scattering Detectors

The sum of the same Pb runs used in the calibration of the forward scattering banks (see section A1a) were used. The single difference data for spectra 3-90 was stored as [.TOTAL]PBSDA and the double difference data as [.TOTAL]PBDDA. The single difference data from detectors 91-134 was stored as [.TOTAL]PBSDB and the double difference data as [.TOTAL]PBDDB.

**A3a** The lengths were calibrated using TRANSFITB1_SUB.COM (spectra 3-90) and TRANSFITB2_SUB.COM (spectra 91-134), Pb run 12570, U run 12571. IP0002.DAT and IP0003.DAT were created using LTCALIB.FOR.

**A3b** The angles (spectra 3-90) were calibrated by:

(1) BCALIB.FOR produces a file with the positions of the 4 longest d spacing Bragg peaks. The output file bcalib.dat was copied to [.data]pb12570b1.dat
(2) ANGLE .FOR calculates the angle with IP0002 and [.data]pb12570b1.dat as input and creates a new IP0002 file with the calibrated angles.

The angles (spectra 91-134) were calibrated by:

(1) BCALIB.FOR produces a file BCALIB.DAT with the positions of the 4 longest d spacing Bragg peaks. The output file bcalib.dat was copied to [.data]pb12570b2.dat. It must be modified by hand to remove the first 90 entries.
(2) ANGLE2.FOR calculates the angle with IP0003 and [.data]pb12570b2.dat as input and creates a new IP0003 file with the calibrated angles.

**A3c** The values of L1 were calibrated by:

Read in [.total]pbsda to workspaces 3-90. Rebin 200 (.5) 456. @PBFIT – output to pbsda.dat. Run L1CAL.FOR on PBSDA.DAT. Create new IP0002 file with new L1 values. Read in [.total]pbsdb to workspaces 1-44. Rebin 200 (.5) 456. @PBFIT – output to PBSDB.DAT. Run L1CAL.FOR on PBSDB.DAT. Create new IP0003 file with new L1 values.

**A3d** The energy and energy resolution were calibrated by running PBFIT.COM and using PBPLOTFIG.FOR to calculate the calibrated values of the final energy and the Gaussian and Lorentzian components of the resolution function. PBPLOTFIG.FOR outputs files E1.DAT, DEG.DAT and DEL.DAT. Mean values of these parameters can be calculated using MEAN1.DAT.

## Appendix 4. File containing mean instrument parameters for forward scattering

Θ is the scattering angle in degrees (section 3d)

$t_0$ is the time of emission of the neutrons from the moderator (section 3a)

$L_0$ is the moderator-sample distance (section 3a)

$L_1$ is the sample-detector distance (section 3c)

$\Phi$ is the azimuthal angle (section 3f)

**EVS$DISK0:[EVSMGR.CALIB.PAR]IP0001.DAT**

| | **Θ (degrees)** | ***$t_0$ (μsec)*** | ***$L_0$ (m)*** | ***$L_1$ (m)*** | ***φ(degrees)*** |
|---|---|---|---|---|---|
| 1 | 6.6563E+01 | -4.0000E-01 | 1.1005E+01 | 5.5370E-01 | 4.1391E+01 |
| 2 | 6.4196E+01 | -4.0000E-01 | 1.1005E+01 | 5.3790E-01 | 3.2529E+01 |
| 3 | 6.2328E+01 | -4.0000E-01 | 1.1005E+01 | 5.3380E-01 | 2.3037E+01 |
| 4 | 6.1108E+01 | -4.0000E-01 | 1.1005E+01 | 5.4150E-01 | 1.3354E+01 |
| 5 | 6.6446E+01 | -4.0000E-01 | 1.1005E+01 | 5.4890E-01 | 3.1987E+02 |
| 6 | 6.4226E+01 | -4.0000E-01 | 1.1005E+01 | 5.3670E-01 | 3.2904E+02 |
| 7 | 6.2349E+01 | -4.0000E-01 | 1.1005E+01 | 5.3260E-01 | 3.3849E+02 |
| 8 | 6.1202E+01 | -4.0000E-01 | 1.1005E+01 | 5.4140E-01 | 3.4817E+02 |
| 9 | 5.7613E+01 | -4.0000E-01 | 1.1005E+01 | 7.5850E-01 | 3.9105E+01 |
| 10 | 5.5469E+01 | -4.0000E-01 | 1.1005E+01 | 7.5140E-01 | 3.2084E+01 |
| 11 | 5.3379E+01 | -4.0000E-01 | 1.1005E+01 | 7.5040E-01 | 2.4913E+01 |
| 12 | 5.1953E+01 | -4.0000E-01 | 1.1005E+01 | 7.5330E-01 | 1.7511E+01 |
| 13 | 5.7722E+01 | -4.0000E-01 | 1.1005E+01 | 7.6320E-01 | 3.2234E+02 |
| 14 | 5.5299E+01 | -4.0000E-01 | 1.1005E+01 | 7.5260E-01 | 3.2903E+02 |
| 15 | 5.3485E+01 | -4.0000E-01 | 1.1005E+01 | 7.4920E-01 | 3.3624E+02 |
| 16 | 4.0052E+01 | -4.0000E-01 | 1.1005E+01 | 7.5450E-01 | 3.4372E+02 |
| 17 | 5.2976E+01 | -4.0000E-01 | 1.1005E+01 | 5.5370E-01 | 4.8994E+01 |
| 18 | 4.8599E+01 | -4.0000E-01 | 1.1005E+01 | 5.3910E-01 | 3.9681E+01 |
| 19 | 4.4966E+01 | -4.0000E-01 | 1.1005E+01 | 5.3380E-01 | 2.9003E+01 |
| 20 | 4.2616E+01 | -4.0000E-01 | 1.1005E+01 | 5.4260E-01 | 1.7014E+01 |
| 21 | 5.3035E+01 | -4.0000E-01 | 1.1005E+01 | 5.5250E-01 | 3.1249E+02 |
| 22 | 4.8623E+01 | -4.0000E-01 | 1.1005E+01 | 5.3910E-01 | 3.2179E+02 |
| 23 | 4.4805E+01 | -4.0000E-01 | 1.1005E+01 | 5.3500E-01 | 3.3236E+02 |
| 24 | 4.2476E+01 | -4.0000E-01 | 1.1005E+01 | 5.4380E-01 | 3.4426E+02 |

| | | | | | |
|---|---|---|---|---|---|
| 25 | 3.8548E+01 | -4.0000E-01 | 1.1005E+01 | 7.4890E-01 | 4.4550E+01 |
| 26 | 4.2424E+01 | -4.0000E-01 | 1.1005E+01 | 7.5740E-01 | 5.2103E+01 |
| 27 | 3.5127E+01 | -4.0000E-01 | 1.1005E+01 | 7.4910E-01 | 3.5713E+01 |
| 28 | 3.2748E+01 | -4.0000E-01 | 1.1005E+01 | 7.5100E-01 | 2.5641E+01 |
| 29 | 4.2827E+01 | -4.0000E-01 | 1.1005E+01 | 7.5610E-01 | 3.0802E+02 |
| 30 | 3.8613E+01 | -4.0000E-01 | 1.1005E+01 | 7.4540E-01 | 3.1506E+02 |
| 31 | 3.5702E+01 | -4.0000E-01 | 1.1005E+01 | 7.4680E-01 | 3.2461E+02 |
| 32 | 3.3046E+01 | -4.0000E-01 | 1.1005E+01 | 7.5210E-01 | 3.3457E+02 |
| 33 | 4.7278E+01 | -4.0000E-01 | 1.1005E+01 | 7.5260E-01 | 1.3435E+02 |
| 34 | 4.3862E+01 | -4.0000E-01 | 1.1005E+01 | 7.4300E-01 | 1.4151E+02 |
| 35 | 4.0825E+01 | -4.0000E-01 | 1.1005E+01 | 7.3730E-01 | 1.4938E+02 |
| 36 | 3.8820E+01 | -4.0000E-01 | 1.1005E+01 | 7.4500E-01 | 1.5859E+02 |
| 37 | 4.7237E+01 | -4.0000E-01 | 1.1005E+01 | 7.5970E-01 | 2.2704E+02 |
| 38 | 4.3832E+01 | -4.0000E-01 | 1.1005E+01 | 7.4420E-01 | 2.2016E+02 |
| 39 | 4.0986E+01 | -4.0000E-01 | 1.1005E+01 | 7.4080E-01 | 2.1188E+02 |
| 40 | 3.8747E+01 | -4.0000E-01 | 1.1005E+01 | 7.4730E-01 | 2.0275E+02 |
| 41 | 5.6329E+01 | -4.0000E-01 | 1.1005E+01 | 5.4660E-01 | 1.3429E+02 |
| 42 | 5.2790E+01 | -4.0000E-01 | 1.1005E+01 | 5.3070E-01 | 1.4369E+02 |
| 43 | 4.9461E+01 | -4.0000E-01 | 1.1005E+01 | 5.2780E-01 | 1.5415E+02 |
| 44 | 4.7332E+01 | -4.0000E-01 | 1.1005E+01 | 5.3540E-01 | 1.6536E+02 |
| 45 | 5.6442E+01 | -4.0000E-01 | 1.1005E+01 | 5.5250E-01 | 2.2658E+02 |
| 46 | 5.2417E+01 | -4.0000E-01 | 1.1005E+01 | 5.3670E-01 | 2.1751E+02 |
| 47 | 4.9440E+01 | -4.0000E-01 | 1.1005E+01 | 5.3150E-01 | 2.0703E+02 |
| 48 | 4.7287E+01 | -4.0000E-01 | 1.1005E+01 | 5.3670E-01 | 1.9591E+02 |
| 49 | 6.1728E+01 | -4.0000E-01 | 1.1005E+01 | 7.5610E-01 | 1.4318E+02 |
| 50 | 6.0190E+01 | -4.0000E-01 | 1.1005E+01 | 7.5020E-01 | 1.5022E+02 |
| 51 | 5.8464E+01 | -4.0000E-01 | 1.1005E+01 | 7.4680E-01 | 1.5712E+02 |
| 52 | 5.7407E+01 | -4.0000E-01 | 1.1005E+01 | 7.5450E-01 | 1.6432E+02 |
| 53 | 6.1868E+01 | -4.0000E-01 | 1.1005E+01 | 7.5860E-01 | 2.1645E+02 |
| 54 | 5.9988E+01 | -4.0000E-01 | 1.1005E+01 | 7.5020E-01 | 2.0973E+02 |
| 55 | 5.8435E+01 | -4.0000E-01 | 1.1005E+01 | 7.4680E-01 | 2.0283E+02 |
| 56 | 5.7260E+01 | -4.0000E-01 | 1.1005E+01 | 7.4850E-01 | 1.9582E+02 |
| 57 | 7.2220E+01 | -4.0000E-01 | 1.1005E+01 | 5.4890E-01 | 1.4232E+02 |
| 58 | 7.0325E+01 | -4.0000E-01 | 1.1005E+01 | 5.3430E-01 | 1.5098E+02 |
| 59 | 6.8708E+01 | -4.0000E-01 | 1.1005E+01 | 5.3260E-01 | 1.6011E+02 |
| 60 | 6.7757E+01 | -4.0000E-01 | 1.1005E+01 | 5.4150E-01 | 1.6926E+02 |
| 61 | 7.2503E+01 | -4.0000E-01 | 1.1005E+01 | 5.5730E-01 | 2.1967E+02 |
| 62 | 7.0732E+01 | -4.0000E-01 | 1.1005E+01 | 5.4150E-01 | 2.1106E+02 |
| 63 | 6.8832E+01 | -4.0000E-01 | 1.1005E+01 | 5.3860E-01 | 2.0201E+02 |
| 64 | 6.7880E+01 | -4.0000E-01 | 1.1005E+01 | 5.4500E-01 | 1.9290E+02 |

## Appendix 5. Resolution of Forward Scattering Detectors

**EVS$DISK0:[evsmgr.calib.par]rp0001.dat**

Δt is the uncertainty in the time of flight measurement in μsec (section 4a).
$\Delta L_0$ is the uncertainty in the incident flight path in cm (section 4a).
$\Delta L_1$ is the uncertainty in the final flight path in cm (section 4b)
EW is the effective width in cm of the detector, used to calculate the angular resolution (Section 4d).
DE1L is the Lorentzian HWHM of the Voigt energy resolution function in meV (section 4c).
DE1G is the Gaussian standard deviation of the Voigt energy resolution function in meV (section 4c).

| | Δt | $\Delta L_0$ | $\Delta L_1$ | EW | DE1L | DE1G |
|---|---|---|---|---|---|---|
| 1 | 3.7000E-01 | 2.1000E+00 | 2.4107E+00 | 2.1742E+00 | 2.9880E+01 | 7.4310E+01 |
| 2 | 3.7000E-01 | 2.1000E+00 | 2.0835E+00 | 1.9567E+00 | 3.0260E+01 | 7.0470E+01 |
| 3 | 3.7000E-01 | 2.1000E+00 | 1.8137E+00 | 1.7701E+00 | 3.0630E+01 | 6.9400E+01 |
| 4 | 3.7000E-01 | 2.1000E+00 | 1.5691E+00 | 1.6234E+00 | 3.1010E+01 | 6.9540E+01 |
| 5 | 3.7000E-01 | 2.1000E+00 | 2.3249E+00 | 2.1076E+00 | 3.2450E+01 | 7.1570E+01 |
| 6 | 3.7000E-01 | 2.1000E+00 | 1.9429E+00 | 1.9178E+00 | 3.4410E+01 | 6.8470E+01 |
| 7 | 3.7000E-01 | 2.1000E+00 | 1.8113E+00 | 1.7258E+00 | 2.6620E+01 | 7.2380E+01 |
| 8 | 3.7000E-01 | 2.1000E+00 | 1.5950E+00 | 1.6006E+00 | 2.8920E+01 | 7.0730E+01 |
| 9 | 3.7000E-01 | 2.1000E+00 | 2.3115E+00 | 2.4156E+00 | 1.6320E+01 | 7.4900E+01 |
| 10 | 3.7000E-01 | 2.1000E+00 | 2.1096E+00 | 2.2009E+00 | 2.2240E+01 | 7.1790E+01 |
| 11 | 3.7000E-01 | 2.1000E+00 | 1.9881E+00 | 2.0057E+00 | 1.6980E+01 | 7.2910E+01 |
| 12 | 3.7000E-01 | 2.1000E+00 | 1.6538E+00 | 1.8686E+00 | 1.7590E+01 | 7.3600E+01 |
| 13 | 3.7000E-01 | 2.1000E+00 | 2.1795E+00 | 2.3234E+00 | 2.1540E+01 | 7.2760E+01 |
| 14 | 3.7000E-01 | 2.1000E+00 | 1.9494E+00 | 2.1714E+00 | 1.1740E+01 | 7.8590E+01 |
| 15 | 3.7000E-01 | 2.1000E+00 | 1.8347E+00 | 1.9753E+00 | 1.6470E+01 | 7.3080E+01 |
| 16 | 3.7000E-01 | 2.1000E+00 | 1.6418E+00 | 1.8238E+00 | 2.4460E+01 | 6.9560E+01 |
| 17 | 3.7000E-01 | 2.1000E+00 | 2.5361E+00 | 2.9942E+00 | 2.2130E+01 | 7.6240E+01 |
| 18 | 3.7000E-01 | 2.1000E+00 | 2.1563E+00 | 2.7613E+00 | 2.4190E+01 | 7.3790E+01 |
| 19 | 3.7000E-01 | 2.1000E+00 | 1.8378E+00 | 2.4393E+00 | 2.4000E+01 | 7.2140E+01 |
| 20 | 3.7000E-01 | 2.1000E+00 | 1.5504E+00 | 2.1106E+00 | 2.2230E+01 | 7.3840E+01 |
| 21 | 3.7000E-01 | 2.1000E+00 | 2.7788E+00 | 2.9707E+00 | 2.4650E+01 | 7.4210E+01 |
| 22 | 3.7000E-01 | 2.1000E+00 | 2.1582E+00 | 2.7170E+00 | 2.5760E+01 | 7.2250E+01 |
| 23 | 3.7000E-01 | 2.1000E+00 | 1.8108E+00 | 2.3809E+00 | 2.2900E+01 | 7.4110E+01 |
| 24 | 3.7000E-01 | 2.1000E+00 | 1.4040E+00 | 2.0765E+00 | 2.5550E+01 | 7.3660E+01 |
| 25 | 3.7000E-01 | 2.1000E+00 | 2.2959E+00 | 3.3746E+00 | 2.6350E+01 | 7.3660E+01 |

| | Δt | $\Delta L_0$ | $\Delta L_1$ | EW | DE1L | DE1G |
|---|---|---|---|---|---|---|
| 26 | 3.7000E-01 | 2.1000E+00 | 2.4347E+00 | 3.5731E+00 | 2.8590E+01 | 6.7000E+01 |
| 27 | 3.7000E-01 | 2.1000E+00 | 1.9867E+00 | 3.1615E+00 | 1.4970E+01 | 6.5030E+01 |
| 28 | 3.7000E-01 | 2.1000E+00 | 1.5138E+00 | 2.9123E+00 | 2.5010E+01 | 7.4070E+01 |
| 29 | 3.7000E-01 | 2.1000E+00 | 2.6861E+00 | 3.5841E+00 | 8.5530E+00 | 6.8980E+01 |
| 30 | 3.7000E-01 | 2.1000E+00 | 2.1895E+00 | 3.3794E+00 | 9.9960E+00 | 8.0590E+01 |
| 31 | 3.7000E-01 | 2.1000E+00 | 1.9135E+00 | 3.1533E+00 | 1.4760E+01 | 7.7220E+01 |
| 32 | 3.7000E-01 | 2.1000E+00 | 1.7985E+00 | 2.8930E+00 | 2.9440E+01 | 7.6970E+01 |
| 33 | 3.7000E-01 | 2.1000E+00 | 2.3666E+00 | 3.1173E+00 | 1.9670E+01 | 7.2520E+01 |
| 34 | 3.7000E-01 | 2.1000E+00 | 2.3387E+00 | 2.9119E+00 | 1.7260E+01 | 7.6610E+01 |
| 35 | 3.7000E-01 | 2.1000E+00 | 1.9754E+00 | 2.7046E+00 | 1.8600E+01 | 7.6650E+01 |
| 36 | 3.7000E-01 | 2.1000E+00 | 1.5929E+00 | 2.4795E+00 | 2.2910E+01 | 7.5540E+01 |
| 37 | 3.7000E-01 | 2.1000E+00 | 2.7653E+00 | 3.2004E+00 | 1.3810E+01 | 7.8830E+01 |
| 38 | 3.7000E-01 | 2.1000E+00 | 2.6627E+00 | 2.9858E+00 | 1.6950E+01 | 8.0050E+01 |
| 39 | 3.7000E-01 | 2.1000E+00 | 2.0752E+00 | 2.7493E+00 | 2.3020E+01 | 7.6490E+01 |
| 40 | 3.7000E-01 | 2.1000E+00 | 1.8098E+00 | 2.4829E+00 | 2.5650E+01 | 7.3320E+01 |
| 41 | 3.7000E-01 | 2.1000E+00 | 2.5857E+00 | 2.7296E+00 | 2.3260E+01 | 7.6120E+01 |
| 42 | 3.7000E-01 | 2.1000E+00 | 2.3646E+00 | 2.4538E+00 | 2.9550E+01 | 7.6090E+01 |
| 43 | 3.7000E-01 | 2.1000E+00 | 1.8678E+00 | 2.1485E+00 | 2.9660E+01 | 6.9740E+01 |
| 44 | 3.7000E-01 | 2.1000E+00 | 1.4766E+00 | 1.8693E+00 | 3.0550E+01 | 7.1390E+01 |
| 45 | 3.7000E-01 | 2.1000E+00 | 2.5933E+00 | 2.7001E+00 | 2.3920E+01 | 7.4710E+01 |
| 46 | 3.7000E-01 | 2.1000E+00 | 2.1579E+00 | 2.4262E+00 | 2.9430E+01 | 7.8800E+01 |
| 47 | 3.7000E-01 | 2.1000E+00 | 1.8118E+00 | 2.1657E+00 | 3.3300E+01 | 7.1530E+01 |
| 48 | 3.7000E-01 | 2.1000E+00 | 1.4504E+00 | 1.8828E+00 | 1.5810E+01 | 6.9050E+01 |
| 49 | 3.7000E-01 | 2.1000E+00 | 2.2574E+00 | 2.1320E+00 | 1.0750E+01 | 7.9420E+01 |
| 50 | 3.7000E-01 | 2.1000E+00 | 2.2306E+00 | 2.0072E+00 | 3.1380E+01 | 7.8990E+01 |
| 51 | 3.7000E-01 | 2.1000E+00 | 1.9359E+00 | 1.8060E+00 | 2.2660E+01 | 6.3830E+01 |
| 52 | 3.7000E-01 | 2.1000E+00 | 1.7579E+00 | 1.7545E+00 | 2.3040E+01 | 7.0660E+01 |
| 53 | 3.7000E-01 | 2.1000E+00 | 2.1214E+00 | 2.1522E+00 | 2.3040E+01 | 7.1140E+01 |
| 54 | 3.7000E-01 | 2.1000E+00 | 2.2152E+00 | 1.9793E+00 | 1.7470E+01 | 7.0070E+01 |
| 55 | 3.7000E-01 | 2.1000E+00 | 1.9061E+00 | 1.9176E+00 | 2.6530E+01 | 7.3550E+01 |
| 56 | 3.7000E-01 | 2.1000E+00 | 1.7279E+00 | 1.8290E+00 | 3.2910E+01 | 6.7380E+01 |
| 57 | 3.7000E-01 | 2.1000E+00 | 2.6325E+00 | 1.7830E+00 | 3.4840E+01 | 7.3460E+01 |
| 58 | 3.7000E-01 | 2.1000E+00 | 2.4864E+00 | 1.6657E+00 | 2.7040E+01 | 6.8450E+01 |
| 59 | 3.7000E-01 | 2.1000E+00 | 2.0912E+00 | 1.5959E+00 | 2.8010E+01 | 7.1980E+01 |
| 60 | 3.7000E-01 | 2.1000E+00 | 1.8609E+00 | 1.4966E+00 | 3.8250E+01 | 6.9490E+01 |
| 61 | 3.7000E-01 | 2.1000E+00 | 2.5727E+00 | 1.8533E+00 | 3.2350E+01 | 6.9100E+01 |
| 62 | 3.7000E-01 | 2.1000E+00 | 2.4350E+00 | 1.7065E+00 | 2.9370E+01 | 6.9590E+01 |
| 63 | 3.7000E-01 | 2.1000E+00 | 2.0013E+00 | 1.6191E+00 | 2.5370E+01 | 7.2370E+01 |
| 64 | 3.7000E-01 | 2.1000E+00 | 1.8858E+00 | 1.5350E+00 | 0.0000E+00 | 7.3460E+01 |

# Appendix 6. Instrument Parameters for Back-Scattering

**File containing instrument parameters for back scattering bank A (S3-S90)**
**EVS$DISK0:[EVSMGR.CALIB.PAR]IP0002.DAT**

| | Θ (degrees) | $t_0$ (μsec) | $L_0$ (m) | $L_1$ (m) |
|---|---|---|---|---|
| 3 | 130.4672 | -0.4157000 | 11.0050 | 0.6747705 |
| 4 | 131.9338 | -0.5338000 | 11.0050 | 0.6716131 |
| 5 | 133.0579 | -0.3363000 | 11.0050 | 0.6588817 |
| 6 | 132.8050 | -0.5144000 | 11.0050 | 0.6642183 |
| 7 | 132.2996 | -0.4171000 | 11.0050 | 0.6686869 |
| 8 | 130.9003 | -0.3913000 | 11.0050 | 0.6882817 |
| 9 | 132.6673 | -0.4923000 | 11.0050 | 0.6574392 |
| 10 | 134.3881 | -0.2896000 | 11.0050 | 0.6410817 |
| 11 | 134.8883 | -0.3632000 | 11.0050 | 0.6379817 |
| 12 | 134.7490 | -0.1396000 | 11.0050 | 0.6374661 |
| 13 | 133.3403 | -0.2885000 | 11.0050 | 0.6579713 |
| 14 | 134.5436 | -0.2448000 | 11.0050 | 0.6318235 |
| 15 | 136.0912 | -0.2145000 | 11.0050 | 0.6213817 |
| 16 | 136.7689 | -0.2530000 | 11.0050 | 0.6192765 |
| 17 | 136.2204 | -0.4242000 | 11.0050 | 0.6294765 |
| 18 | 134.9788 | -0.3489000 | 11.0050 | 0.6433660 |
| 19 | 136.0485 | -0.4401000 | 11.0050 | 0.6207287 |
| 20 | 137.6185 | -0.5180000 | 11.0050 | 0.6130078 |
| 21 | 138.3813 | -0.4554000 | 11.0050 | 0.6082869 |
| 22 | 137.7410 | -0.4583000 | 11.0050 | 0.6155922 |
| 23 | 138.8744 | -0.4107000 | 11.0050 | 0.5977131 |
| 24 | 140.3823 | -0.3490000 | 11.0050 | 0.5882974 |
| 25 | 140.5575 | -0.2599000 | 11.0050 | 0.5903713 |
| 26 | 139.3308 | -0.3506000 | 11.0050 | 0.6017765 |
| 27 | 140.8276 | -0.3650000 | 11.0050 | 0.5800183 |
| 28 | 142.3703 | -0.3504000 | 11.0050 | 0.5734869 |
| 29 | 142.3065 | -0.4941000 | 11.0050 | 0.5804765 |
| 30 | 141.2702 | -0.3881000 | 11.0050 | 0.5856817 |
| 31 | 143.4913 | -0.3519000 | 11.0050 | 0.5631026 |
| 32 | 145.1110 | -0.2379000 | 11.0050 | 0.5534869 |
| 33 | 144.1598 | -0.3988000 | 11.0050 | 0.5636817 |
| 34 | 146.1180 | -0.3570000 | 11.0050 | 0.5460026 |
| 35 | 147.3548 | -0.2592000 | 11.0050 | 0.5426713 |
| 36 | 146.3615 | -0.4036000 | 11.0050 | 0.5507922 |
| 37 | 148.2314 | -0.4020000 | 11.0050 | 0.5336131 |
| 38 | 149.7075 | -0.3803000 | 11.0050 | 0.5331713 |
| 39 | 148.6062 | -0.4816000 | 11.0050 | 0.5371026 |

| | Θ (degrees) | $t_0$ (μsec) | $L_0$ (m) | $L_1$ (m) |
|---|---|---|---|---|
| 40 | 151.9368 | -0.3536000 | 11.0050 | 0.5180922 |
| 41 | 151.8600 | -0.4475000 | 11.0050 | 0.5234922 |
| 42 | 154.6504 | -0.2809000 | 11.0050 | 0.5028974 |
| 43 | 154.6273 | -0.3985000 | 11.0050 | 0.5092869 |
| 44 | 160.2468 | -0.4253000 | 11.0050 | 0.4892026 |
| 45 | 157.5291 | -0.4026000 | 11.0050 | 0.4985870 |
| 46 | 162.8277 | -0.4781000 | 11.0050 | 0.4800235 |
| 47 | 130.7935 | -0.4309000 | 11.0050 | 0.6771497 |
| 48 | 132.1970 | -0.4634000 | 11.0050 | 0.6642183 |
| 49 | 133.1700 | -0.3188000 | 11.0050 | 0.6544765 |
| 50 | 133.0489 | -0.2729000 | 11.0050 | 0.6551817 |
| 51 | 132.0011 | -0.4248000 | 11.0050 | 0.6699026 |
| 52 | 130.6237 | -0.3840000 | 11.0050 | 0.6881765 |
| 53 | 132.9112 | -0.4945000 | 11.0050 | 0.6541392 |
| 54 | 134.3012 | -0.4116000 | 11.0050 | 0.6416131 |
| 55 | 136.4848 | -0.4116000 | 11.0050 | 0.6400000 |
| 56 | 134.4089 | -0.3321000 | 11.0050 | 0.6421713 |
| 57 | 132.9198 | -0.3318000 | 11.0050 | 0.6580870 |
| 58 | 134.5938 | -0.4649000 | 11.0050 | 0.6356288 |
| 59 | 135.9571 | -0.5556000 | 11.0050 | 0.6284183 |
| 60 | 136.7983 | -0.2545000 | 11.0050 | 0.6180713 |
| 61 | 136.0501 | -0.3665000 | 11.0050 | 0.6256869 |
| 62 | 134.4992 | -0.3263000 | 11.0050 | 0.6414817 |
| 63 | 136.3356 | -0.4233000 | 11.0050 | 0.6170288 |
| 64 | 138.0733 | -0.3684000 | 11.0050 | 0.6061869 |
| 65 | 138.5809 | -0.3978000 | 11.0050 | 0.6038817 |
| 66 | 137.9523 | -0.3006000 | 11.0050 | 0.6089713 |
| 67 | 139.0672 | -0.5083000 | 11.0050 | 0.5971235 |
| 68 | 140.2882 | -0.5126000 | 11.0050 | 0.5912974 |
| 69 | 140.2659 | -0.4646000 | 11.0050 | 0.5921922 |
| 70 | 139.0866 | -0.4323000 | 11.0050 | 0.6020765 |
| 71 | 140.9989 | -0.4637000 | 11.0050 | 0.5778288 |
| 72 | 142.5156 | -0.4291000 | 11.0050 | 0.5735869 |
| 73 | 142.4799 | -0.3962000 | 11.0050 | 0.5736817 |
| 74 | 141.0699 | -0.3945000 | 11.0050 | 0.5859765 |
| 75 | 144.1488 | -0.4040000 | 11.0050 | 0.5579078 |
| 76 | 145.0556 | -0.3986000 | 11.0050 | 0.5585660 |
| 77 | 143.7413 | -0.5344000 | 11.0050 | 0.5675921 |
| 78 | 146.2234 | -0.4686000 | 11.0050 | 0.5451078 |
| 79 | 147.2485 | -0.4711000 | 11.0050 | 0.5453765 |
| 80 | 146.3060 | -0.4652000 | 11.0050 | 0.5520660 |
| 81 | 148.8123 | -0.4765000 | 11.0050 | 0.5318131 |
| 82 | 149.8621 | -0.4177000 | 11.0050 | 0.5295817 |

| | Θ (degrees) | $t_0$ (μsec) | $L_0$ (m) | $L_1$ (m) |
|---|---|---|---|---|
| 83 | 148.7900 | -0.4213000 | 11.0050 | 0.5366660 |
| 84 | 151.8867 | -0.5311000 | 11.0050 | 0.5160235 |
| 85 | 152.1363 | -0.3597000 | 11.0050 | 0.5181765 |
| 86 | 154.6800 | -0.4205000 | 11.0050 | 0.5011183 |
| 87 | 154.6256 | -0.4639000 | 11.0050 | 0.5099765 |
| 88 | 157.3379 | -0.4516000 | 11.0050 | 0.4983869 |
| 89 | 160.3500 | -0.5154000 | 11.0050 | 0.4863183 |
| 90 | 163.1410 | -0.5037000 | 11.0050 | 0.4784183 |

**File containing instrument parameters for back-scattering bank B (S91-S134)**
**EVS$DISK0:[EVSMGR.CALIB.PAR]IP0002.DAT**

| | Θ (degrees) | $t_0$ (μsec) | $L_0$ (m) | $L_1$ (m) |
|---|---|---|---|---|
| 1 | 131.1180 | -0.6588000 | 11.00500 | 0.6301287 |
| 2 | 132.8132 | -0.3635000 | 11.00500 | 0.6030974 |
| 3 | 133.4570 | -0.4430000 | 11.00500 | 0.6007869 |
| 4 | 133.4908 | -0.3817000 | 11.00500 | 0.6006713 |
| 5 | 132.2988 | -0.5920000 | 11.00500 | 0.6180869 |
| 6 | 130.6160 | -0.6493000 | 11.00500 | 0.6358183 |
| 7 | 133.5822 | -0.4639000 | 11.00500 | 0.5983922 |
| 8 | 134.9576 | -0.3802000 | 11.00500 | 0.5833765 |
| 9 | 135.3030 | -0.4799000 | 11.00500 | 0.5829765 |
| 10 | 134.5561 | -0.4859000 | 11.00500 | 0.5903765 |
| 11 | 133.1175 | -0.6038000 | 11.00500 | 0.6081921 |
| 12 | 135.1621 | -0.5336000 | 11.00500 | 0.5838974 |
| 13 | 136.5101 | -0.4918000 | 11.00500 | 0.5707870 |
| 14 | 137.0373 | -0.5299000 | 11.00500 | 0.5665817 |
| 15 | 136.5596 | -0.4027000 | 11.00500 | 0.5724504 |
| 16 | 136.5596 | -0.4027000 | 11.00500 | 0.5519000 |
| 17 | 136.8396 | -0.5283000 | 11.00500 | 0.5668079 |
| 18 | 138.5584 | -0.4716000 | 11.00500 | 0.5546660 |
| 19 | 138.9462 | -0.4753000 | 11.00500 | 0.5503713 |
| 20 | 138.1395 | -0.4711000 | 11.00500 | 0.5572765 |
| 21 | 139.3408 | -0.5241000 | 11.00500 | 0.5432974 |
| 22 | 141.0563 | -0.3655000 | 11.00500 | 0.5331661 |
| 23 | 140.8032 | -0.4541000 | 11.00500 | 0.5337817 |
| 24 | 139.2979 | -0.4404000 | 11.00500 | 0.5434870 |
| 25 | 141.6319 | -0.4829000 | 11.00500 | 0.5280921 |
| 26 | 143.1375 | -0.4551000 | 11.00500 | 0.5212556 |
| 27 | 142.7428 | -0.5454000 | 11.00500 | 0.5253661 |
| 28 | 141.2269 | -0.5099000 | 11.00500 | 0.5330817 |
| 29 | 136.5242 | -0.5099000 | 11.00500 | 0.6334428 |

| | Θ (degrees) | $t_0$ (μsec) | $L_0$ (m) | $L_1$ (m) |
|---|---|---|---|---|
| 30 | 145.4173 | -0.4245000 | 11.00500 | 0.5015712 |
| 31 | 144.2731 | -0.4412000 | 11.00500 | 0.5120660 |
| 32 | 146.7183 | -0.5599000 | 11.00500 | 0.4965817 |
| 33 | 147.6929 | -0.4808000 | 11.00500 | 0.4921713 |
| 34 | 146.5414 | -0.4208000 | 11.00500 | 0.4962713 |
| 35 | 149.0569 | -0.5661000 | 11.00500 | 0.4833026 |
| 36 | 150.2828 | -0.4207000 | 11.00500 | 0.4788608 |
| 37 | 148.8338 | -0.4926000 | 11.00500 | 0.4860765 |
| 38 | 152.6647 | -0.4804000 | 11.00500 | 0.4676765 |
| 39 | 152.1087 | -0.5366000 | 11.00500 | 0.4680922 |
| 40 | 155.0412 | -0.5211000 | 11.00500 | 0.4562869 |
| 41 | 154.7799 | -0.4774000 | 11.00500 | 0.4562817 |
| 42 | 157.3462 | -0.5290000 | 11.00500 | 0.4479922 |
| 43 | 160.8082 | -0.5002000 | 11.00500 | 0.4342974 |
| 44 | 163.5115 | -0.5027000 | 11.00500 | 0.4271026 |

## Other Instrument Parameters

**Single difference measurements**

| Detector group | 3-46 | 47-90 | 91-132 |
|---|---|---|---|
| $E_1$ (meV) | 4897.4 (6) | 4897.8 (7) | 4895.5 (4) |
| $\Delta E_{1L}$ (meV) | 134 (2) | 142 (2) | 147.5 (1.3) |
| $\Delta E_{1G}$ (meV) | 55 (2) | 54 (2) | 48 (3) |

**Double difference measurements**

| Detector group | 3-46 | 47-90 | 91-132 |
|---|---|---|---|
| $E_1$ (meV) | 4898.7 ± 0.5 | 4899.7 ± 0.7 | 4896.9 ± 0.4 |
| $\Delta E_{1L}$ (meV) | 33 ± 2 | 41 ±3 | 47 ± 2 |
| $\Delta E_{1G}$ (meV) | 93 ± 2 | 88 ± 2 | 85 ± 2 |

| Detector group | 3-46 | 47-90 | 91-132 |
|---|---|---|---|
| $\Delta t$ (μsec) | 0.36 (2) | 0.32 (2) | 0.34 (3) |
| $\Delta L$ (cm) | 3.22 (8) | 3.46 (9) | 3.10 (9) |

**References**


1 *Theory of Neutron Scattering from Condensed matter Volume 1*, S W Lovesey, (Oxford University Press 1984) section 3.4

2 *The measurement of anomalous neutron inelastic cross-sections at electronvolt energy transfers*. J Mayers and T Abdul-Redah, J. Phys. Condens. Matter 16 (2004) 4811–4832

3 *Measurement of momentum distributions of light atoms and molecules in condensed matter systems using inelastic neutron scattering. C Andreani, D Colognesi, J Mayers and G Reiter. Adv Phys **54** 377-469 (2005)*

4 *Excess of proton mean kinetic energy in supercooled water.* A Pietropaolo, R Senesi, C Andreani et al. *Phys. Rev. Lett. **100** 127802 (2008).*

5 *Proton momentum distribution in liquid water from room temperature to the supercritical phase.* C. Pantalei, A. Pietropaolo, R. Senesi, S. Imberti, C. Andreani, J. Mayers, C. Burnham, and G. Reiter. *Phys. Rev. Lett. **100** 177801 (2008)*

6 *Measurement of the kinetic energy and lattice constant in hcp solid helium at temperatures 0.07-0.4K.* M Adams and J Mayers *Phys. Rev. Lett. **98** 85301(2007)*

7 *Quantum and classical relaxation in the proton glass.* Y. Feng, C. Ancona-Torres et al. *Phys. Rev. Lett. **97** 69901 (2006)*

8 *Anomalous behaviour of proton zero point motion in water confined in carbon nano-tubes.* G. Reiter, C. Burnham et al *Phys. Rev. Lett. **97** 247801 (2006)*

9 *Proton momentum distribution in a protein hydration shell.* R. Senesi, A. Pietropaolo et al. *Phys. Rev. Lett. **98** 138102 (2007)*

10 *Measurement of the 3-D Born-Oppenheimer potential of a proton in a hydrogen-bonded system via deep inelastic neutron scattering.* D Homouz, G. Reiter et al. *Phys. Rev. Lett **98** 115502 (2007)*

11 *Calibration of the electron volt spectrometer, a deep inelastic neutron scattering spectrometer at the ISIS pulsed neutron spallation source.* A. L. Fielding and J. Mayers, *Nucl. Inst. Meth. A*, **480**, 680 (2002)

12 *Advances on detectors for low-angle scattering of epithermal neutrons* E P Cippo, G Gorini, M Tardocchi, et al. Measurement Science and Technology **19** 47001 (2008)

13 *YAP Scintillators for resonant detection of epithermal neutrons at pulse neutron sources.* M. Tardocchi, G. Gorini et al. *Rev. Sci. Inst.* **75,** 4880 (2004).

14 *A resonant detector for high-energy inelastic neutron scattering experiments.* C. Andreani, A. Pietropaolo et al. Applied Physics Letters **85** 5454 (2004)

15 *Foil cycling technique for the VESUVIO spectrometer operating in the resonance detector configuration,* E M Schoonveld, J. Mayers et al Rev. Sci. Inst. **77** 95103 (2006)
Author(s): Schooneveld EM, Mayers J, Rhodes NJ, et al.
16 *Resolution function in deep inelastic neutron scattering using the Foil Cycling Technique.* A. Pietropaolo, C. Andreani et al Nuc. Inst Meth A **570** 498 (2007)
17 *Double Difference method to improve the resolution of an eV neutron spectrometer.* P.A. Seeger, A.D. Taylor and R. M. Brugger, *Nucl. Instr. Methods* **A 240**, 98 (1985)
18 *Neutron Cross Sections* ,S.F. Mughabghab, (Academic Press, Orlando, Florida, 1984)
19 *Initial State Effects in Deep Inelastic Neutron Scattering.* J Mayers, C Andreani, G Baciocco, *Phys Rev B* **39** 2022 (1989)
20 To be published
21 *Multiple scattering in deep inelastic neutron scattering: Monte Carlo simulations and experiments at the ISIS eVS inverse geometry spectrometer* J. Mayers, A.L. Fielding, R. Senesi. Nucl. Inst Meth. **A 481**, 454 (2002)
22 *Pulsed Neutron Scattering*, C. Windsor, (Taylor and Francis, London, 1981).